JGR Planets

RESEARCH ARTICLE
10.1029/2022JE007504

Groundwater-Controlled Deposition of Equatorial Layered Deposits in Central Arabia Terra, Mars

I. Di Pietro[1,2], G. Schmidt[3], A. C. Tangari[1], F. Salese[4], S. Silvestro[5,6], A. G. Fairén[4,7], L. Marinangeli[1], and M. Pondrelli[8]

[1]Remote Sensing and Planetology Laboratory, Università Gabriele D'Annunzio, Chieti, Italy, [2]Now at Italian Space Agency, Roma RM, Italy, [3]GeoQuTe Lab, Roma Tre University, Rome, Italy, [4]Centro de Astrobiologia CSIC-INTA, Madrid, Spain, [5]Istituto Nazionale di Astrofisica (INAF), Napoli, Italy, [6]Carl Sagan Center, SETI Institute, Mountain View, CA, USA, [7]Cornell University, Ithaca, NY, USA, [8]International Research School of Planetary Sciences, Università d'Annunzio, Pescara, Italy

Key Points:

- Regional groundwater fluctuations influenced the deposition, mineralogy, and preservation of Equatorial Layered Deposits (ELDs) in Arabia Terra
- Four different stratigraphic sequences of layered deposits have been identified on the basis of strata thickness and attitude
- Mineralogical analyses of ELDs suggest the presence of different levels of hydration of sulfates

Supporting Information:

Supporting Information may be found in the online version of this article.

Correspondence to:

I. Di Pietro,
ilaria.dipietro@unich.it

Citation:

Di Pietro, I., Schmidt, G., Tangari, A. C., Salese, F., Silvestro, S., Fairén, A. G., et al. (2023). Groundwater-controlled deposition of Equatorial Layered Deposits in central Arabia Terra, Mars. *Journal of Geophysical Research: Planets*, *128*, e2022JE007504. https://doi.org/10.1029/2022JE007504

Received 23 JUL 2022
Accepted 28 FEB 2023

Author Contributions:

Conceptualization: I. Di Pietro, G. Schmidt, F. Salese, L. Marinangeli, M. Pondrelli
Formal analysis: G. Schmidt
Investigation: I. Di Pietro, G. Schmidt, A. C. Tangari, F. Salese
Methodology: I. Di Pietro, A. C. Tangari, M. Pondrelli
Supervision: M. Pondrelli
Visualization: I. Di Pietro, G. Schmidt
Writing – original draft: I. Di Pietro, G. Schmidt

Abstract Equatorial Layered Deposits (ELDs) reveal aspects of past depositional environments useful for timing climatic and geological events on Mars. However, their formation has several contending hypotheses which reflect a diverse range of possible environments. To better constrain their formation mechanism, we analyzed the stratigraphic and mineralogical characteristics and mapped the distribution of ELDs within three close craters, Sera, Jiji, and an unnamed crater in central Arabia Terra. Analyses of craters' geology allowed us to reconstruct the paleo-environments where ELDs have been deposited. Thinning and thickening sequence trends show shared and repeated variations in the depositional environment, reflecting sediment accumulation strongly controlled by a regional groundwater reservoir. Layered deposits are characterized by monohydrated and polyhydrated sulfate signatures implying an interaction between water and rock in acidic conditions. Our study contributes to the understanding of regional geological processes in Arabia Terra revealing long-term aqueous activity.

Plain Language Summary Despite years of orbital observations of the surface of Mars, mid-to low-latitude layered deposits (LD) in Arabia Terra are not yet fully understood. These deposits record an important geological sequence of the early Martian history, but their exact formation, specifically the putative role of the water in their formation and preservation, remains an unanswered question. This study helps in further understanding these processes by comparing and contrasting LD present in craters in very close proximity to each other. In this way, proposed hypotheses benefit from having a control that is not limited to a singular crater or location. Our study contributes to the understanding of regional geological processes in Arabia Terra revealing long-term aqueous activity. Results combine various analyses, including measurements of layer thickness and attitudes, orbital spectroscopy, basin geometry, and morphologies aimed at reconstructing the geological evolution of the area. In particular, we interpreted that LD were emplaced in a depositional environment reflecting sediment accumulation strongly controlled by a regional groundwater reservoir in acidic conditions.

1. Introduction

Martian layered deposits (LD) have been extensively recognized in a considerable range of geomorphic settings within Mars' equatorial regions, including crater basins (e.g., Le Deit et al., 2013; Murana, 2018; Pondrelli et al., 2019; Zabrusky et al., 2012), the chasmata of Valles Marineris and chaotic terrains (e.g., Al-Samir et al., 2017; Baioni & Tramontana, 2017; Davis et al., 2018; Fueten et al., 2017; Glotch & Rogers, 2007; Noel et al., 2015; Schmidt et al., 2018), intercrater plains of Meridiani Planum and Arabia Terra (e.g., Grotzinger et al., 2005; Malin & Edgett, 2001; McLennan et al., 2005; Pondrelli et al., 2015), and in the southern hemisphere within the intercrater plains on the northern rim of Hellas basin (e.g., Ansan et al., 2011; Bernhardt et al., 2016; Day et al., 2016; Salese, Ansan, et al., 2016; Wilson et al., 2007). These deposits have been informally designated as "Equatorial Layered Deposits" (ELDs), a term that collectively indicates the light-toned LD found in the aforementioned wide range of geological contexts in the equatorial regions of Mars. ELDs are thought to be Late Noachian to Hesperian in age and were deposited on the older, cratered Noachian crust (e.g., Hynek & Phillips, 2008; Le Deit et al., 2008; Pondrelli et al., 2015; Poulet et al., 2008). They typically have a light-toned appearance with repetitive bedding and they are thought to be fine-grained and weakly lithified, due to the formation of a variety of

Writing – review & editing: G. Schmidt, A. C. Tangari, F. Salese, S. Silvestro, A. G. Fairén, L. Marinangeli, M. Pondrelli

erosional morphologies (e.g., Andrews-Hanna et al., 2010; Fergason & Christensen, 2008; Lewis et al., 2008; Zabrusky & Andrews-Hanna, 2010). Furthermore, the observed amounts of eroded ELD that could have been removed from basins, combined with the lack of significant talus nearby eroded outcrops, point toward a grain size that can be transported by aeolian processes (e.g., Fergason & Christensen, 2008; Hynek et al., 2002; Kite & Mayer, 2017). Layering generally has sub-horizontal dips, but there are exceptions such as Danielson crater where some layers are inclined up to 25° nearby slopes (Lewis & Aharonson, 2014; Murana, 2018). ELDs are also known for their association with hydrated minerals such as clays and sulfates and may reach several kilometers in thickness at places (Murchie, Roach, et al., 2009; Poulet et al., 2005; Zabrusky et al., 2012). Over the past decades, many scenarios have been proposed to explain both the voluminous layered deposition and their aqueous alteration history. Most prior studies considered the LD as members of a single rhythmic orbital facies with large-scale stratigraphic correlations (Grotzinger & Milliken, 2012), but the depositional origin of such facies is still debated. A wide range of other depositional environments have also been suggested for the ELDs, reflecting the great variability of the geological context in which they were formed.

Proposed formational hypotheses include groundwater moderated aeolian loess (Andrews-Hanna & Lewis, 2011; Andrews-Hanna et al., 2007, 2010; Annex & Lewis, 2020; Bridges & Muhs, 2012; Cadieux & Kah. 2015; Grotzinger et al., 2005; Kite, Halevy, et al., 2013; Kite, Lewis, et al., 2013; Murchie, Roach, et al., 2009; Zabrusky et al., 2012) or pyroclastic deposits (Hynek et al., 2002; Kerber et al., 2012; Scott & Tanaka, 1982); groundwater-fed evaporitic playa deposits (Andrews-Hanna & Lewis, 2011; Andrews-Hanna et al., 2007; Zabrusky et al., 2012), spring deposits or mud volcanoes deposits (Franchi et al., 2014; Pajola et al., 2022; Pondrelli et al., 2011, 2015, 2019; Rossi et al., 2008); lacustrine deposits (Fueten et al., 2017; Lucchitta et al., 1992; Mangold et al., 2020; Newsom et al., 2003; Salese, Kleinhans, et al., 2020); ground ice melt-driven cemented deposits (Cadieux & Kah, 2015; Niles & Michalski, 2009); sub-ice volcanic flow deposits (Chapman & Tanaka, 2002; Komatsu et al., 2004); weathered basalts (Madden et al., 2004); other mixed-aeolian deposits (Day & Catling, 2020; Michalski & Niles, 2012; Tanaka, 2000); impact base surge deposits (Knauth et al., 2005).

Regardless of their exact origin, such widespread and copious presence of LD in the geological record all over the martian surface indicates a global sedimentological response to changes in climatic conditions and hence, depositional processes. The use of orbital images is typically insufficient to define discrete depositional models alone (Edgett & Malin, 2002; Grotzinger et al., 2011; Zabrusky et al., 2012); however, the stratigraphic analysis of LD may reveal crucial constraints on depositional models. In fact, the analysis of sedimentary basin architecture, layer thicknesses, and trends may be interpreted in terms of potential accommodation space and water base level variation.

Bedding is the main feature of sedimentary deposits, representing a layer that can be clearly distinguished (lithologically, structurally, texturally, etc.) from layers above and below. At the small scale, a singular bed reflects change in depositional conditions: sediment input/rate erosion, environment energy, sediment competence (Christie-Blick & Driscoll, 1995). At a wider scale, a stratal packaging reflects the interaction between sediment input, accommodation space, and base level. In this light, ELDs provide an exceptional opportunity to analyze stratal patterns, looking for evidence of local or regional drivers of sedimentation and sediment preservation.

With this aim, we focused on three craters: Sera, Jiji and an unnamed crater (UC) (also indicated as "UC" in this paper) (Arabia Terra region; Figure 1) based on the presence of ELDs coupled with their unique proximity to each other and the regional scenario extensively hosting LD in a wide range of geological contexts to be further compared with the study area. Selection of the region of interest was bolstered by the availability of both High Resolution Imaging Science Experiment (HiRISE) stereo-pairs and CRISM (Compact Reconnaissance Imaging Spectrometer for Mars) observations allowing detailed analyses. Sera is a ~30 km diameter, about 1 km deep, impact crater (1°3′27″W, 8°49′39″N) in Arabia Terra. Jiji is located ~15 km west of Sera, is ~21 km in diameter, and centered at 1°44′21″W, 8°46′2″N. Sera shares a similar floor elevation to Jiji, although the latter is unique in that its impact affected the southeast rim of an already present UC (~28 km in diameter; 1°52′33″W, 9°1′58″N), forming a much larger and connected basin. The study area is located within the 1:5,000,000 scale quadrangle MC-11 (Oxia Palus) (Wilhelms, 1976). Nevertheless, deposits such as Arabia Terra region sediments are predicted to be genetically related and widespread across much of Meridiani Planum (Andrews-Hanna et al., 2010; Grotzinger et al., 2005) where analyses performed by Mars Exploration Rover missions provide significant ground truth (Figure 1b). Arabia Terra is also closely linked to the ancient fluvial catchment of Coogoon Valles (Molina et al., 2017) that includes the target (i.e., Oxia Planum; Figure 1b) the ExoMars mission (Vago et al., 2015).

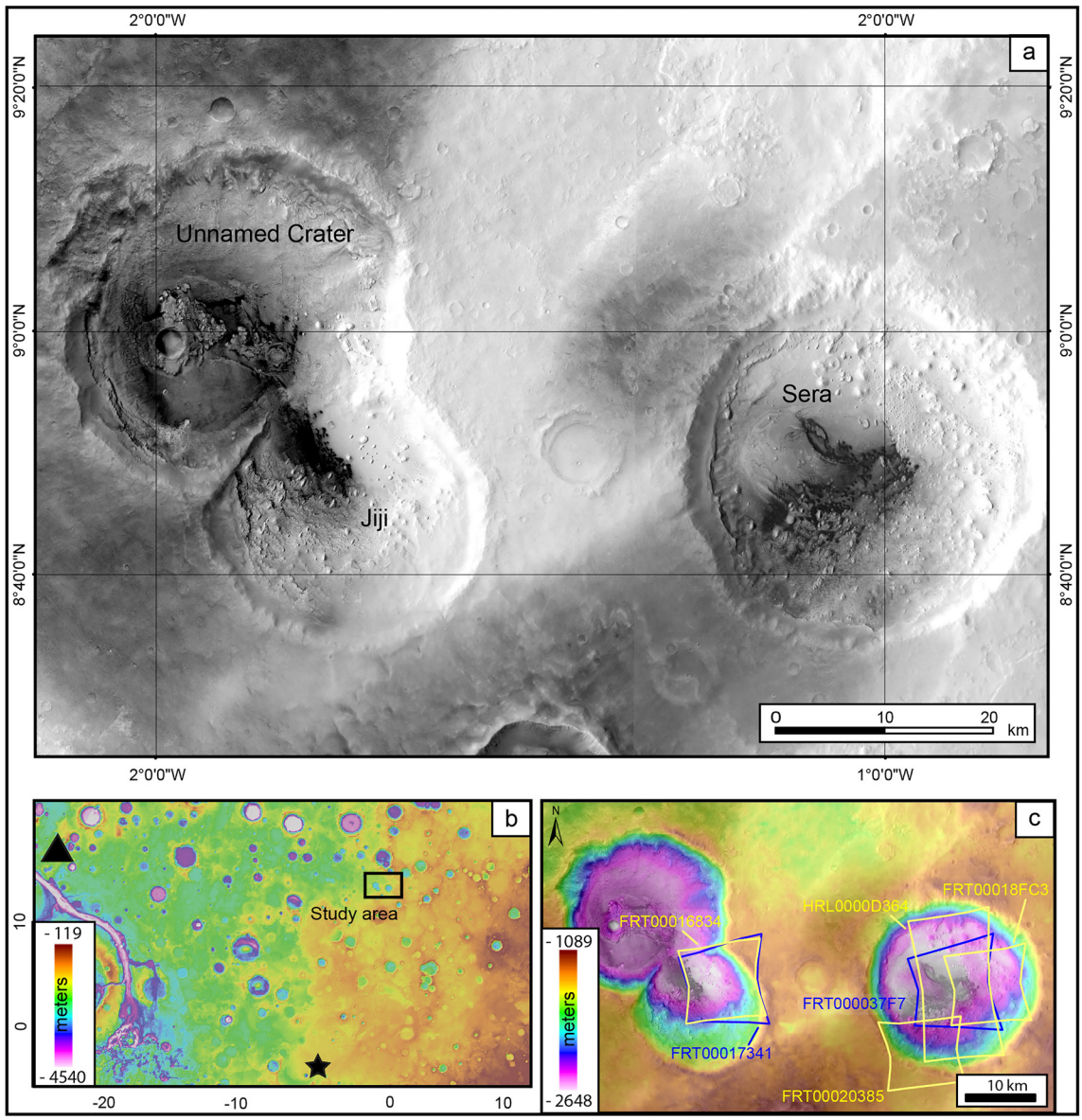

Figure 1. Reference figure of study area. (a) High-Resolution Stereo Camera (HRSC) mosaic showing the two craters in a simple cylindrical coordinate system. (b) MOLA-colorized (Mars Orbiter Laser Altimeter) digital elevation model (DEM) showing the location of the study area. The black star marks the Mars Exploration Rover-B landing site. The black triangle marks the Oxia Planum region (ExoMars landing site). (c) Topography of the study area by HRSC DEM with footprints of analyzed Compact Reconnaissance Imaging Spectrometer for Mars observations.

The complexity and variability of the ELDs requires detailed studies to better understand the depositional processes, environments, controls and their implications on the relative climatic conditions. In particular, Koeppel et al. (2022), pairing observations of low bedding inclinations, low cohesion, regionally extensive sequences, and the presence of LD outside topographic lows, interpreted ELDs in the same study area to result from airfall processes and intermittent wetting.

In this study, we analyzed and correlated the stratigraphic sequences in the three basins in order to test the presence of common trends and to infer the nature of the controls on deposition reaching slightly different conclusions from Koeppel et al. (2022). We also addressed the nature of the aqueous alteration which affected the ELDs. Our aim was to reconstruct the geological history at the local scale by distinguishing different deposits and mapping their geometry and lateral distribution to be used as stratigraphic correlation tools in other moderately sized basins of the Arabia Terra region. Eventually, Arabia Terra is perfectly suitable to investigate ELDs due to their

significant and widespread presence, the high variability of settings in which they are found, and the extensive evidence of aqueous alteration in the geological evolution of the region. Arabia Terra could also be considered as an optimal key transitional terrain due to the lack of a northward sharp elevation variation and could make it more feasible to define the interaction between sedimentary deposits and groundwater processes (see Section 2).

2. Background

Arabia Terra represents a pivotal area to better understand and characterize the origin of ELDs and their global geological importance. Layered deposits have been found both within the intracrater basins and in the intercrater plains along with exceptional geological variability of settings (i.e., morphological associations, geometries of the deposits/basins, sedimentary structures, and mineralogy) (e.g., Allen & Oehler, 2008; Franchi et al., 2014; Oehler & Allen, 2010; Pondrelli et al., 2011, 2015, 2019; Zabrusky et al., 2012) through the use of the Mars Orbiter Camera, Context Camera (CTX) and HiRISE high-resolution images (Malin, 2000; Malin & Edgett, 2001; Malin et al., 2007; McEwen et al., 2007). This region is thought to have undergone significant resurfacing in the Late Noachian (Hynek & Phillips, 2001).

Although it was originally considered as a part of the cratered highlands (Greeley & Guest, 1987; Scott & Tanaka, 1986), more recent data showed lower values of topography and crustal thickness (Zuber, 2001) and a slightly different fluvial dissection than what is typical of highland terrains (Balme et al., 2020; Davis et al., 2016, 2019; Hynek & Phillips, 2001). Indeed, Arabia Terra has an elevation variation, crustal thickness, and character distinct from both the younger northern lowlands and the southern highlands (Andrews-Hanna et al., 2008). Nevertheless, it shows a wide mineralogical diversity, recording evidence of a prolonged interaction between water and the Martian sedimentary deposits throughout the Noachian and early Hesperian epochs. In fact, over the past decades, many hypotheses have been proposed to describe the aqueous alteration history in Arabia Terra (McCollom & Hynek, 2005; Squyres & Knoll, 2005; Squyres et al., 2004, 2009). Many authors have also suggested a remarkable control by groundwater processes in the area (Andrews-Hanna & Lewis, 2011; Andrews-Hanna et al., 2007, 2010; Franchi et al., 2014; Oehler & Allen, 2010; Pondrelli et al., 2015; Rossi et al., 2008; Salese et al., 2019; Zabrusky et al., 2012). In particular, monohydrated and polyhydrated sulfates were detected in association with most of the ELDs (Bibring et al., 2006; Gendrin et al., 2005; Mangold et al., 2008) using visible/near infrared imaging spectroscopy from the Observatoire pour la Minéralogie, l'Eau, les Glaces et l'Activité (OMEGA) on board the ESA Mars Express mission (Bibring et al., 2005) and from the CRISM on board the NASA Mars Reconnaissance Orbiter mission (Murchie et al., 2007). While hydrated sulfates accompanying the ELDs are accepted (Wiseman et al., 2010), the extent to which water contributed to their deposition is still debated. Indeed, ELDs originating under persistent, water-stable conditions (Pondrelli et al., 2019; Wiseman et al., 2010; Zabrusky et al., 2012) as well as following only short interactions with water (Kite, 2019; Koeppel et al., 2022) have both been proposed in the last few years.

3. Methodology

The morphology, stratigraphy, topography, and mineralogy of Sera and Jiji were analyzed at different resolutions.

Visible imagery at multiple scales was used to reconstruct the stratigraphy of the studied region. The CTX camera (6 m/pixel) (Malin et al., 2007) and the HiRISE camera (25 cm/pixel) (McEwen et al., 2007) provided detailed images which were useful to investigate target morphologies. CTX images provided a full coverage of the study area to be compared with High-Resolution Stereo Camera (HRSC) (Neukum & Jaumann, 2004) digital elevation model (DEM) which provided the topographic base map with a spatial resolution of 50 m/pixel. The regional topographic context was given by the Mars Orbiter Laser Altimeter (MOLA; Smith et al., 2001) with a 463 m/pixel spatial resolution. CTX and HiRISE stereo-pair images were first radiometrically corrected and projected using the USGS software ISIS3 (Integrated Software for Imagers and Spectrometers (ISIS)) and then processed to produce DEMs through the NASA Ames Stereo Pipeline (Broxton & Edwards, 2008; Moratto et al., 2010; Shean et al., 2016). The resulting CTX and HiRISE DTMs have a minimum gridding of 6 and 1 m/pixel, respectively, and were used to reconstruct stratigraphic relationships and for detailed layering analyses. Processed HiRISE and CTX stereo-pairs are listed in Table S1 of Supporting Information S1. Mars Odyssey (ODY) Thermal Emission Imaging System (THEMIS) daytime and night-time infrared (IR) images (100 m/pixel; Christensen et al., 2004) were also used to preliminarily investigate the thermophysical properties of the units of interest.

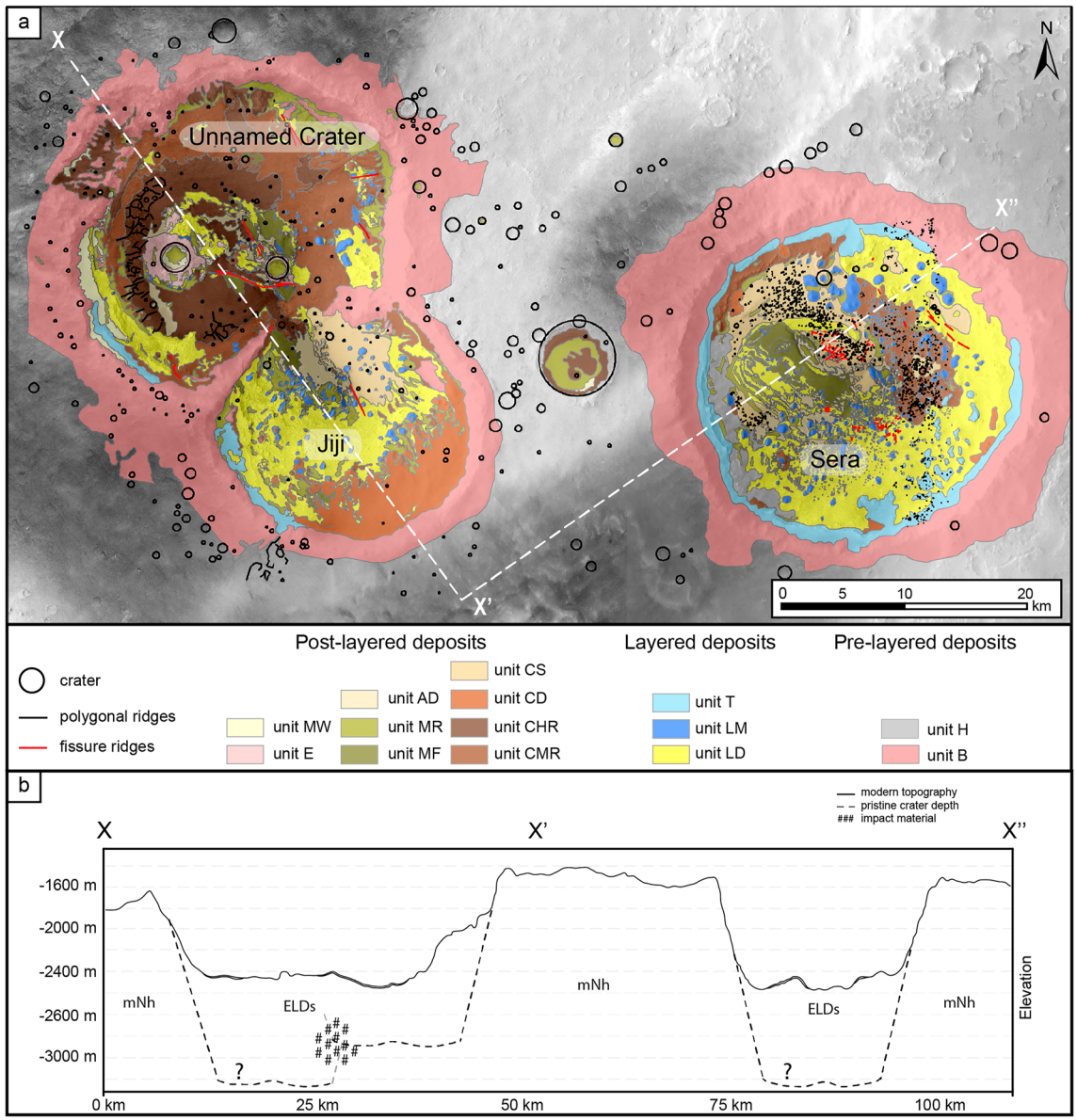

Figure 2. Geologic map of the study area over High-Resolution Stereo Camera images (H5242_0000; H5260_0000). Equatorial Layered Deposits (ELDs) are represented by layered deposits (LD—yellow) and layered mounds (LM—blue). X-X′ represent the cross section used for the block diagram in the discussion section. Pre-layered deposits: bedrock (B), hummocky deposits (H). LD: LD, LM, flat-terraced units (T). Post-layered deposits: medium rugged cover (CMR), high rugged cover (CHR), dusty cover (CD), smooth cover (CS), fossil megaripples (MF), recent megaripples (MR), aeolian deposits (AD) (i.e., dunes and dust) (AD), ejecta (E), mass wasting deposits (MW). (b) Cross section X-X″ shows the putative basin infill between the modern topography (solid line) and the inferred geometry after the impact (dashed line) computed using the methods described in Garvin et al. (2003) and measured in the HRSC-based digital elevation model. mNh = Middle Noachian Highland unit (Tanaka et al., 2014). Question marks represent the uncertainty to establish if the ELDs entirely fill the two basins down to the pristine crater floor.

We produced a geologic map of Sera and Jiji (Figure 2) based on a 6 m/pixel CTX mosaic; the geological units were mapped based on the surface's texture, as well as their relief and albedo following the same methodology used in Salese, Di Achille, et al. (2016), Di Pietro et al. (2018), and Ruj et al. (2017).

The mapping area is enclosed in latitudes ranging from 8°30′ to 9°20′N and longitudes ranging from 0°44′ to 2°10′W, considering a simple cylindrical coordinate system. We used a combination of different criteria to identify the geological units, including (a) main characteristics (i.e., morphology and topography), (b) surface properties (e.g., rough or smooth surface, albedo, etc.), and (c) orbital facies (e.g., layering, bedforms, etc.) observed both at the CTX and, when available, at the HiRISE scale. Once identified, geological units were named based on their most prominent morphological criteria. Crosscutting relationships were used to correlate and infer

relative stratigraphic relations. There are a large number of linear features visible at HiRISE scale; however, they are not all shown in the main map to keep it as uniform as possible since the spatial accuracy/data availability between CTX and HiRISE are extremely variable throughout the study area.

Hyperspectral data from the CRISM instrument were used to analyze the mineralogy of the LD. We analyze CRISM images (Figure 1c) listed in Table S1 of Supporting Information S1, including Full Resolution Targeted (FRT) and Half Resolution Long Targeted (HRL) images in the wavelength interval between the visible and near infrared (0.36–2.6 μm) (Murchie et al., 2007; Murchie, Seelos, et al., 2009). The FRT observations show a spatial resolution of 18 m/pixel covering ≈100 km^2, whereas Half Resolution Targeted (HRL) images show a spatial resolution of 40 m/pixel covering ≈200 km^2. Ultimately, only the observations FRT000037F7, FRT000018FC3, and FRT00016834 are presented due to a layer of dust that covers the interior of the craters impeding the extraction of reliable spectra in the other observations (Mangold et al., 2009). Compact Reconnaissance Imaging Spectrometer for Mars data were processed using the Analysis Tool CAT 7.1.1 developed for the ENVI© software (Murchie, Seelos, et al., 2009) following the method described in Flahaut et al. (2015). Atmospheric absorptions were removed using the scaled volcano-scan method described by McGuire et al. (2009). The CRISM data set was subsequently cleaned of noise using destriping and despiking algorithms of the CIRRUS tool included in CAT (Itok & Parente, 2021). The "spectral smile" correction has also been applied, according to the method described in Murchie et al. (2007). Analytical phase identification of the mineralogical composition was carried out by recognizing the regions of interest (ROIs) and extrapolating the significant spectra from there. These spectra were first ratioed by the flat neutral spectra coming from homogeneous areas near the ROI and then compared to the pure minerals within the RELAB and USGS spectral libraries (Clark et al., 1990; Kokaly et al., 2017). Specifically, the spectra presented in the results comprised of averages of 10's of pixels from chosen ROI (ROI), in an effort to reduce noise. Mafic and sulfates minerals were mapped using the spectral CRISM parameters (Pelkey et al., 2007; Viviano et al., 2014). Mafic minerals have been better identified in the CRISM image FRT000037F7 than its partial overlapping FRT00018CF3 where poor quality of the image did not allow for extrapolation of a good spectral result. First order identification of these minerals in the CRISM data is accomplished through the computation of the spectral parameters proposed by Viviano et al. (2014) (i.e., OLINDEX3, LCPINDEX2, and HCPINDEX2) allowing us to identify the spectral signatures of mafic minerals such as olivine, low-calcium pyroxene and high calcium pyroxene respectively (Viviano et al., 2014). Generally, olivine shows some spectral signatures near 0.65 μm and broad absorption features from 1.0 μm to 1.25 (Chukanov, 2014; Clark et al., 1990). Pyroxene is spectrally identified by absorptions at 1.0 and 2.0 μm (Klima et al., 2007; Skok et al., 2012). On the other hand, sulfates were identified using the computation of the spectral parameters BD1900_2, BD2100_2, and SINDEX, which provide an estimate of the 1.9 μm absorption indicating the fundamental vibration of the water molecule (Clark et al., 1990; Flahaut et al., 2015; Hunt, 1970), 2.1 and 2.4 μm band depth respectively (Bishop et al., 2009). Concerns that any detections related to the sulfates presented could in part be influenced by the so called "spurious absorptions" (Leask et al., 2018), an artifact that mimics absorptions at 1.9 and 2.1 μm, have been addressed in two ways. First, we compared pixels between two separate observations (FRT000037F7 and HRL0000D364) and then by taking ratios of the radiance of columns associated with individual pixels. Since HRL000D364 and FRT000037F7 cover the same area, HRL000D364 was used as a reference to reliability of the observed absorptions and avoidance of artifacts.

Remote sensing methods of measuring layers using Martian orbital data have been previously implemented across Mars in both Valles Marineris and Arabia Terra (Annex & Lewis, 2020; Fueten et al., 2008, 2014; Lewis et al., 2008; Schmidt et al., 2018, 2021). We expand upon the layer thickness measurements from Schmidt et al. (2021) of five HiRISE DEMs (Sera, Jiji and UC pedestal crater) and one CTX DEM (UC) (Table S1 in Supporting Information S1) by correlating thinning and thickening sequences between the craters, as well as presenting a more detailed analysis of fold structures observed in the layer attitude measurements. Layer thicknesses were obtained by measuring elevation and distance between each layer along a line parallel to the slope following the method of Schmidt et al. (2018, 2021) and Fueten et al. (2014, 2008). The resulting measurements had an average error of ±0.4 m due to both the vertical resolution of the DEMs (<0.5 m McEwen et al., 2007; Sutton et al., 2022) and erosion of the layer edges (Annex & Lewis, 2020; Schmidt et al., 2021). The quality of the CTX measurements has been controlled in the area where the HiRISE stereo-pair used in Jiji overlaps the CTX stereo-pair (Table S1 in Supporting Information S1). The CTX measurements did not deviate substantially from those taken from the exact locations in the HiRISE DEM. We focused on ensuring that both transects and point placement were acceptable. Points were placed on the layer edges along the transect, which is parallel to the dip

direction. The elevation difference of the two points is then a value for the layer thickness. Careful attention to point placement is given using 3D scenes to ensure that points are not placed on erosional surfaces. When necessary, dips were corrected by multiplying the tangent of the dip angle by the horizontal distance between two adjacent layer edges, and then subtracting the vertical distance between the two-layer edges (Schmidt et al., 2021). Multiple transects were measured within each HiRISE image. A total of 530 layer thickness measurements were taken along 115 transects. A total of 474 layer attitudes were obtained using the Orion software (Pangaea Scientific, 2006) and plotted on Schmidt-nets. Orion determines the best-fit plane of a layer based on the elevation values of points placed on the edge of the layer. Attitudes are generally determined using 7–15 points spaced <100 m apart. Dips are corrected following the method of Schmidt et al. (2021).

4. Results

4.1. Geological Mapping

The geologic map (Figure 2) shows the vertical and lateral distribution of the deposits within the study area. We divided the stratigraphic sequence and informally named the observed units; however, we also refer to previous literature when possible (Hynek & Di Achille, 2017; Tanaka et al., 2014). We mainly focused on LD rather than other units that were not the target of this work. Sera, Jiji and UC are about 30, 21, and 28 km in diameter respectively. Their inferred geometry after the impact is computed using Garvin et al. (2003) and an HRSC-based DEM (Figure 2b and Table S1 in Supporting Information S1). Despite the awareness of the intrinsic limitations of this methodology due to the difficulty to precisely estimate the original crater geometry—as well as the amount of eroded material—we estimated an order of magnitude of the basins infill thicknesses less than ∼1 km for Sera and UC, while it is less than ∼600 m for Jiji (Figure 2b; Table S1 in Supporting Information S1).

4.1.1. Pre-Layered Deposit Units

ELDs lie on the Middle Noachian Highland unit (mNh) according to the global-scale Mars geologic map (Tanaka et al., 2014) or in terrains mapped as "Cratered unit" (Nhc1), "Subdued cratered unit" (Nhc2), "Highly eroded crater unit" (C1) and "Moderately eroded crater unit (C2)," in more recent, detailed geological mapping (Hynek & Di Achille, 2017). They consist of medium albedo, relatively smooth materials, with sharp edges and steep margins that suggest resistance to weathering and erosion. These deposits may be a mixture of volcanic deposits, impact breccias, impact-related melted sheets and erosional deposits of Noachian age (Hynek & Di Achille, 2017). In western Sera, we also distinguished hummocky deposits (H) since their recognition was straightforward. Since they were not the focus of our study, we grouped most of the pre-layered deposits as "bedrock" (B), which can be found almost exclusively at crater rims.

4.1.2. Layered Deposits

Previously indicated as the undivided etched unit (HNMu) in Hynek and Di Achille (2017), LD entirely and unconformably fill the craters on the top of B in the study area.

We distinguished between LD (Figure 3a) and layered mounds (LM) (Figure 3b). Both units consist of meter(s)-thick well-bedded light-toned layers with intermediate surface roughness originating from a stair-step erosional topography, and show a light-toned appearance at both CTX and HiRISE scales (Figure 3), showing sinuous margins and undulated surfaces at places cut by quasi-circular depressions (Figure 3a).

Repetitive horizontal to sub horizontal bedding (Figures 3a and 3b) is observed, and beds are disrupted in meter-scale polygonal features at high-resolution (Figure 3h).

Layered mounds form in lateral continuity with LD (Figures 3b and 3c) and consist of deposits that are texturally indistinguishable from LD except for the morphology that they are associated with. Both circular and elongated LM are observed with sizes from tens to hundreds of meters; however, no consistent preferential orientation is observed. Apical pits are not observed on the top of the mounds as well as specific textures (i.e., breccia).

Layered deposits are covered by aeolian dust or coverage deposits at places (Figures 3b and 3e). In particular, the deepest portion of the Sera basin is represented by a flat surface with a constant elevation between −2,575 and −2,550 m. We consider this surface as the top of the strata of underlying LD covered by a dark and very thin deposit (CS, i.e., smooth cover) (Figures 3g and 3h). The typical polygonal pattern of LD is observed in patches or is faintly visible below CS at the HiRISE scale (Figure 3g). This surface is heavily affected by hundreds

10.1029/2022JE007504

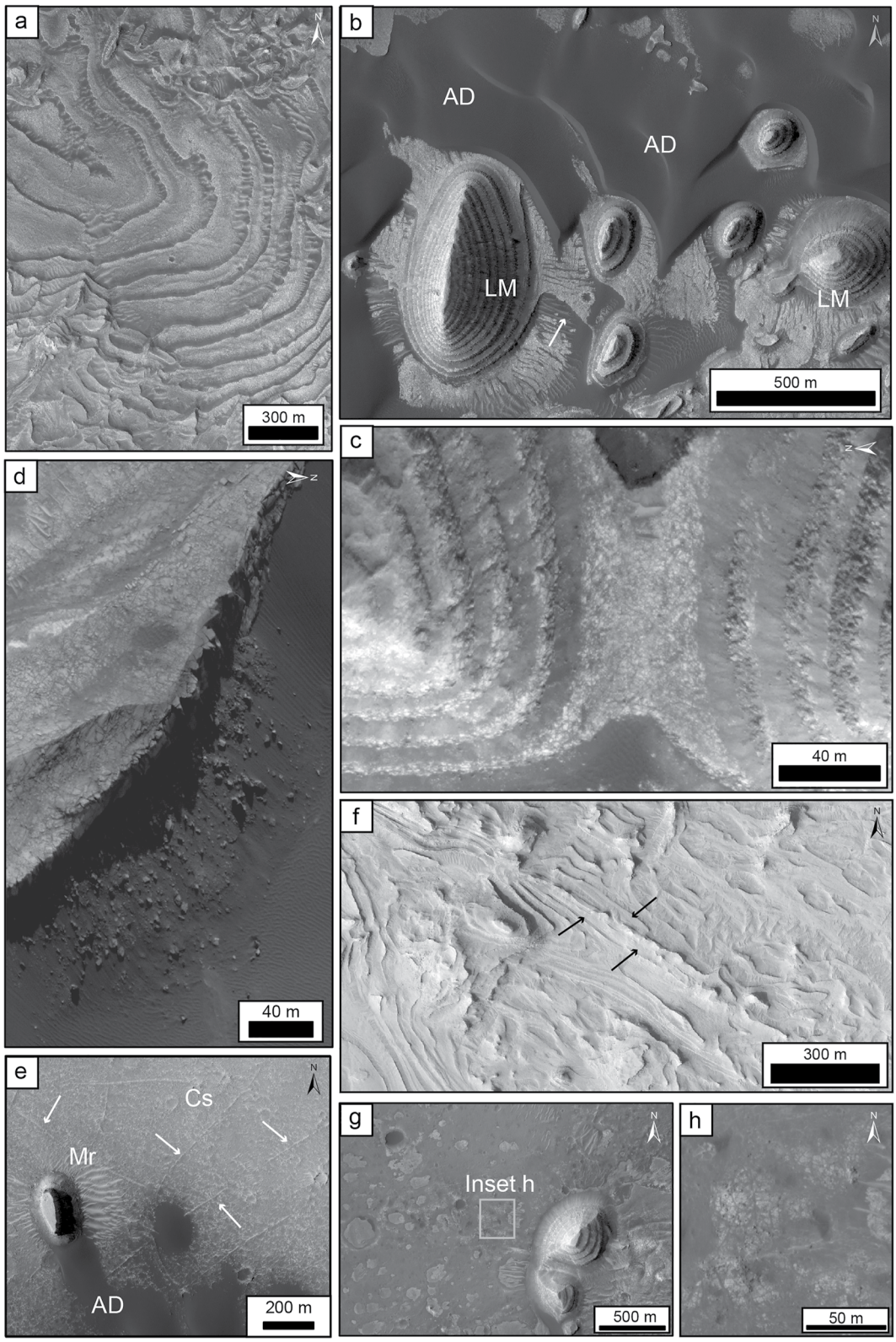

Figure 3.

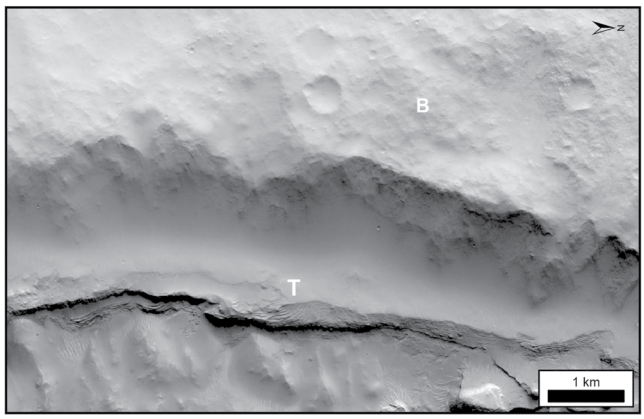

Figure 4. Flat surface *T* encompasses Sera crater ≈500 m below the inner rim and locally displays sub-horizontal layers. B = bedrock (i.e., undifferentiated pre-layered deposits). CTX image P02_001625_1901 (central coordinates: 1°15′50,664″W 8°48′38,62″N).

of small craters (<300 m in diameter) visible at the HiRISE scale, while it appears slightly smoother at the CTX scale due to CS deposition (Figure 3e) that covers the crater floor.

Sets of linear features have been identified to affect the flat surface (Figure 3e). The preferential orientations are about NW–SE and NE–SW, crossing each other. Each linear feature shows two parallel ridges with a meter-scale spacing (<3 m) extending over hundreds of meters; their overall expression is in relief, but the troughs between parallel ridges are not resolvable even at the HiRISE DTM scale.

Meter-scale polygonal features are also identified both in the dome inlier and eastern scarp (Figure 3d) of Sera crater, as well as angular blocks transported downslope from the disrupted edges of the scarp (Figure 3d). Because of these characteristics, we consider Sera central dome as made of LD, even if these deposits are partially covered by dust.

At places, LD are associated with linear features with positive topography (Figure 3f). The orientation is variable, although a rough NW–SE trend is observed for most of the features. The straight shape of these structures suggests that they are controlled by tectonics and are composed of materials that are resistant to the erosion. The upwelling of fluid flow through syn-sedimentary faults/fractures may explain the positive relief (Bargar, 1978); hence, they can be considered as impact-related fracturing features, that is, fissure ridges. Clastic dykes may also explain these kind of features as they form in response to over-pressured and fluidized materials moving upward and creating a geometric pattern (Hurst et al., 2011). However, since the two processes are difficult to distinguish one from another and since the formation mechanism of these features do not substantially influence the geological evolution of our target deposits (ELDs), we hereafter consider them as fissure ridges without further discussion.

We also recognized a terrace-like deposit showing a flat surface (*T*) which has been included in the LD since it locally displays sub-horizontal layers (Figure 4). This unit has not been merged with LD or LM since the surface is smoother and relatively darker at the CTX scale and no significant bedforms or meter-scale polygonal features are observed compared to LM and LD. Some aeolian covers (e.g., transverse aeolian ridges; Balme et al., 2008) with a spacing of tens of meters are visible on the HiRISE scale. *T* encompasses Sera crater ≈500 m below the inner rim (Figure 4) and 100–150 m below the Jiji rim. In Sera, the top surface of unit *T* decreases in elevation from −1,900 to −2,250 m north-westward. Possibly due to the limited extent in the western portions of both Jiji and UC and their shallower depth, a smaller elevation gap is observed (from −1,900 to −1,750 m). There is no clear geometric correlation with crater rims and/or Arabia Terra north-decreasing topography (Hynek & Phillips, 2008) since the Sera rim/plateau is almost constant for the whole crater (≈−1,500 m), while the Jiji rim is almost absent due to the erosion/superposition with the pre-existent northern crater. Isolated and/or dustier eroded patches of deposit *T* are present in south/south-eastern Sera and western Jiji, suggesting this deposit was more laterally extended once.

4.1.3. Post-Layered Deposit Units

The stratigraphic sequence in the study area is capped by mass wasting (unit MW) deposits along crater walls, secondary crater ejecta (unit E), coverages and aeolian deposits (AD) whether fossil (i.e., lithified) (MF) or loose (MR, AD) (Figure 5). Although, we are aware that the classification of aeolian linear features has become more complex in the last years (Balme et al., 2008; Hugenholtz et al., 2017; Milliken et al., 2014; Montgomery et al., 2012), we distinguished two generations of these bedforms which have been simplified just into fossil (i.e., lithified) and recent (i.e., loose) megaripples (MF and MR, respectively).

Figure 3. Layered deposits (LD). (a) Southern LD (High Resolution Imaging Science Experiment (HiRISE) image: ESP_022116_1890). (b) Layered mounds (LM) and dark dune deposits (aeolian deposits) (HiRISE image: PSP_002047_1890). The white arrow shows evidence of lateral continuity between LD and mounds. (c) Lateral continuity and polygonal pattern of two LM (HiRISE image: PSP_002047_1890). (d) Close up of the polygonal pattern at the eastern scarp of the layered dome in Sera crater (HiRISE image: PSP_002047_1890). (e) Unit CS covering the layered Sera crater floor. White arrows mark the set of linear features faintly visible below CS (HiRISE image: PSP_002047_1890). (f) Linear features in correspondence to LD (HiRISE image: ESP_047421_1890). (g) CS pre-dating Sera LM but covering the crater floor in LD. (h) Close up of the white box in panel (g) showing the polygonal pattern below the dark and thin deposit CS.

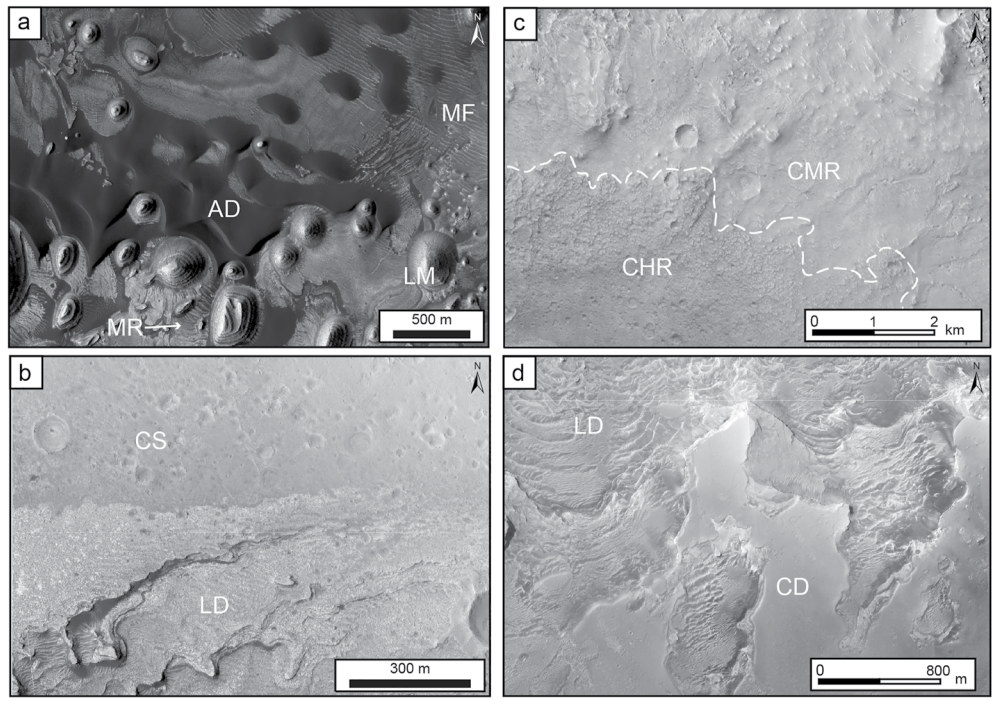

Figure 5. Post-layered deposits. (a) Aeolian bedforms represented by (from the oldest to the youngest deposit) fossil megaripples (MF), recent megaripples (MR) and dark dust and dunes (aeolian deposits) (High Resolution Imaging Science Experiment (HiRISE) image PSP_002047_1890). (b) Dark-toned coverage (CS) superposed on Equatorial Layered Deposits in Sera. (c) High rugged (CHR) and medium rugged cover (CMR) (CTX image G01_018714_1888). (d) Layered deposits overlapped by CD unit in Jiji crater (HiRISE image ESP_069234_1890).

Fossil megaripples (MF) are brighter at both the CTX and HiRISE scales and are unconformably found on the top of LD. They show very narrow crests that reach up to 10 m in height and have a 20 m spacing. The orientation of these aeolian bedforms is mainly ≈NW–SE in the whole study area (Figure 5a).

Several coverage units post-date the LD (Figure 5) with a thickness that can be generally estimated in few meters or less. These thin deposits unconformably onlap on and post-date ELDs. In particular, the deepest portion of the Sera basin is covered by a very thin deposit (CS, i.e., smooth cover) that is medium light-toned at the CTX scale. On the other hand, at HiRISE scale, it is slightly darker (Figures 3e and 5b) the typical exiguous thickness of these deposits makes possible to observe (fainted below CS) the polygonal pattern (Figures 3h and 3i) on which CS unconformably lie.

High rugged cover (CHR) and medium rugged cover (CMR) deposits (Figure 5c) are two coverage units that disconformably lie above ELDs. At the CTX scale, CHR is more rugged, more resistant to weathering and erosion, and with a slightly lower albedo than CMR. The high rugged cover unconformably covers CMR as well as the LD.

CD consists of very dusty and smooth material (Figure 5d) that shows no significant bedforms or any other features at CTX scale, whereas sparse small craters (tens of meters) and recent aeolian bedforms are observed at HiRISE scale. It mostly outcrops in S-SE Jiji.

The most recent deposits in the study area are represented by recent (i.e., loose) megaripples (MR) and dark loose AD (Figure 5a). Recent megaripples are abundant, but not ubiquitously distributed. They preferentially form close to friable LD or mounds. The average spacing between two crests is of tens of meters (20–30 m). Their preferential orientation is generally ≈NE–SW (Figure 5a), although it may change at places (e.g., around LM, Figure 5c) AD are dark in color in both CTX and HiRISE imagery and mainly found in the topographic lows. The AD unit is represented mostly by both mere dust accumulation and lunate structures with arcuate slip faces (i.e., barchan dunes), reaching more than 10 m in height and showing meter-scale ripples visible on their stoss side in HiRISE imagery.

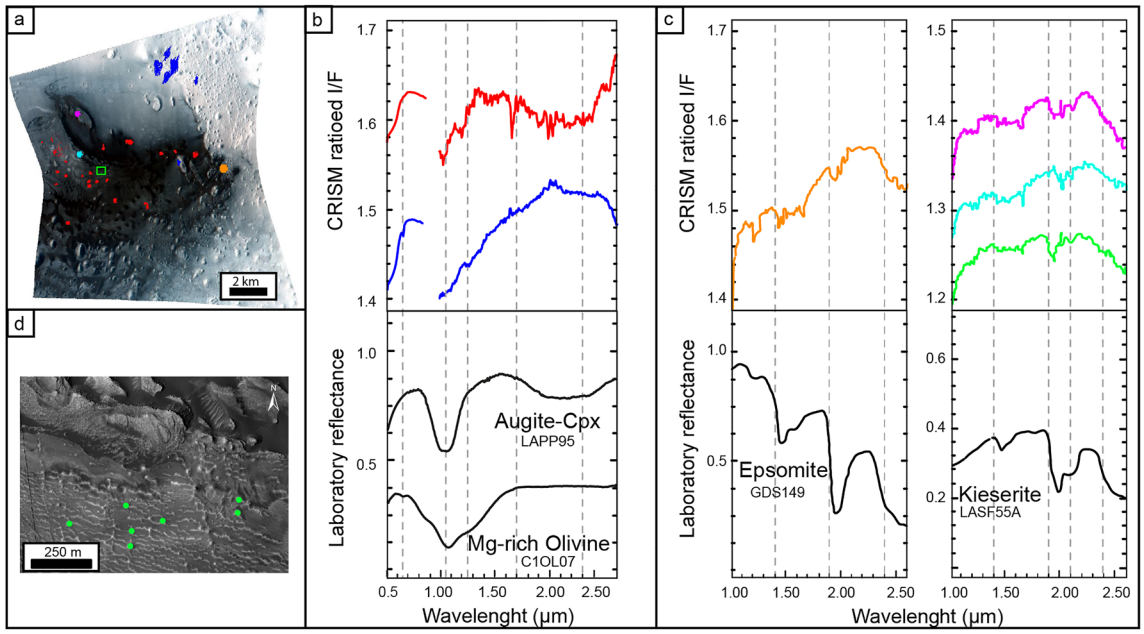

Figure 6. Ratioed IR analyses of Compact Reconnaissance Imaging Spectrometer for Mars (CRISM) observations FRT000037F7 of Sera crater. (a) False color composite of CRISM observation FRT000037F7 (R = 2.5 μm, G = 1.5 μm, B = 1.1 μm). The regions of interest (ROI) are color-coded to match the spectral signatures in panels (b and c). (b) Ratioed spectra of mafic minerals extracted from the blue and red ROIs compared with laboratory spectra (RELAB spectral library). (c) CRISM ratioed spectra of sulfates are color-coded to match the ROIs in panel (a) and compared with the reflectance spectra measured in laboratory (RELAB and USGS spectral libraries). (d) High Resolution Imaging Science Experiment imagery of small mounds indicating the location (green circle) of kieserite (spectra showed in panel (c)). Each green dot represents small areas of one to three pixels. A zoomed view of these small mounds is provided in Figure 12.

4.1.4. Mineralogical Composition

Compact Reconnaissance Imaging Spectrometer for Mars spectra extracted from different areas of Sera (Figures 6 and 7) show the occurrence of mafic minerals and hydrated minerals such as sulfates.

Specifically, two different ROIs were defined (blue and red) among mafic minerals (Figure 6a). The blue ROI on the surface of the ELD showed spectral absorptions of 0.65 μm and a broad absorption signature from 1.05 to 1.25 μm indicative of olivine. These spectral signatures match well with Mg-rich olivine reference spectra such as forsterite (Mg_2SiO_4) (Figure 6b). The red ROI identified on the bulge and dark aeolian material generally exhibits a broad spectral feature near 1 μm and from ≈2.0 to ≈2.5 μm suggesting the occurrence of pyroxene such as augite ($(((Ca,Mg,Fe,Ti,Al)_2(Si,Al)_2(O)_6)$) (Figure 6b).

Diagnostic spectral signatures in the 1.4–2.4 μm wavelength interval indicative of hydrated minerals such as sulfates have been identified in the ELDs within Sera and Jiji craters (Figures 6a, 6c, 6d, and 7). Specifically, the spectral data extrapolated from the ROIs for all analyzed CRISM images (Figures 6 and 7) exhibit absorption bands at 1.4 and 1.9 μm indicating the fundamental vibration of the H_2O molecule. This is also very close to 2.1 and 2.4 μm, suggesting the presence of mono-hydrated sulfates such as kieserite ($MgSO_4H_2O$). Compact Reconnaissance Imaging Spectrometer for Mars observation FRT000037F7 shows a stronger 1.9 μm absorption feature and a broad absorption between 1.4 and 1.6 μm (orange ratioed spectra Figure 6c) which might indicate the occurrence of polyhydrated sulfate such as epsomite ($MgSO_4{\cdot}7\ H_2O$), in addition to the kieserite (Figure 6c). The mixture of poly- and mono-hydrated sulfates in the layered sequence of the Sera-Jiji area was also indicated by Koeppel et al. (2022). There appears to be a topographic trend between kieserite and epsomite outcrops where kieserite characterizes lower elevations between −2,600 and −2,450 m while epsomite occurs at elevations above −2,400 m (Figure 6). However, the limited number of spectral occurrences and the CRISM spatial resolution do not allow more detailed analysis in the study area.

4.2. Layer Measurements

Layering—suitable for measurements—is mostly concentrated in the southwest areas of the craters and gradually tapers north and south along the crater walls (Figure 2). In Jiji, they do not form central mounds as observed in

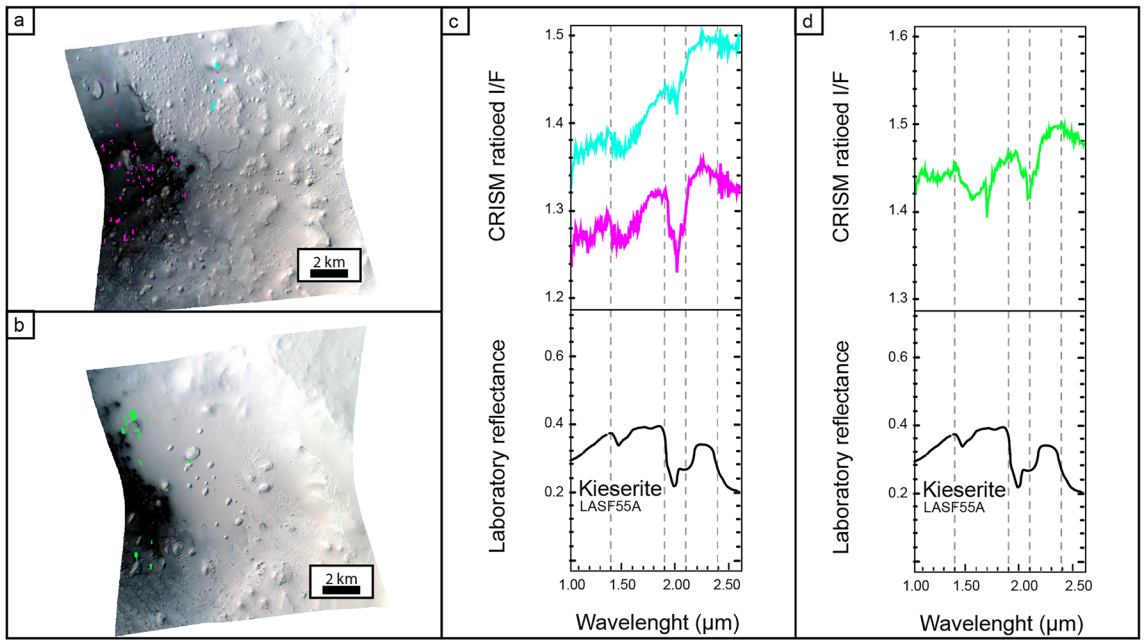

Figure 7. Ratioed IR analyses of Compact Reconnaissance Imaging Spectrometer for Mars (CRISM) observations. (a) False color composite of CRISM FRT000018FC3 in Sera crater (R: 2.5 μm; G: 1.5 μm; B: 1.1 μm) with the location of sulfate-rich regions shown by regions of interest (ROIs) cyan and fuchsia in color. (b) False color composite of CRISM FRT00016834 in Jiji crater (R: 2.5 μm; G: 1.5 μm; B: 1.1 μm) with the location of sulfate-rich regions shown by ROIs green in color. Panels (c and d) ratioed spectra extracted from the ROIs compared with spectra of sulfates from the spectral library used as reference (RELAB spectral library).

other basins on Mars (Kite, Halevy, et al., 2013; Kite, Lewis, et al., 2013; Le Deit et al., 2013), whereas there is a topographical dome of LD in the center of Sera.

We measured the thickness of 530 layers which showed several shared attributes between craters, including thinning and thickening sequences within the ELDs (Figure 8). As discussed previously in Schmidt et al. (2021), the ELDs in Sera (Figure 9a) and Jiji (Figure 9b) show similarity in layer thickness range and thickness average as well as total deposit thickness. However, Jiji contains ≈130 m more of observable layering to measure at the uppermost elevations of the deposit (Figure 8). The ELDs of UC mapping site (Figure 1) lack the same distribution (both horizontally and vertically) as the others, however it has an identical layer thickness average as the ELD of Jiji and Sera. In general, Sera tends to show less variation in elevation than Jiji. Basic correlations show a lower sequence "A" (≈150 m thick), a middle sequence "B" (≈200 m thick), an upper sequence "C" (≈100–120 m thick), and a final sequence "D" (≈50 thick) (Figure 8). Sequences were correlated by counting repeated peak average thicknesses which are labeled A1, A2, A3, B1, B2, B3, C1, C2, C3, and D, etc (Figure 8). We included layer thickness measurements of the layered deposit around the secondary crater of UC despite consisting of a pedestal crater deposit which typically have exhumed layering (Komatsu et al., 2007). Although both the layer thickness average and range of the pedestal crater deposit (located in UC) are similar to the other ELDs in the study area, it is unlikely to share an origin. This was done to better constrain the possibility of it being related to the ELDs observed elsewhere in the mapping area.

A total of 474 layer attitudes were measured revealing dips ranging from horizontal to 40°. Layers generally did not show a uniform dip direction. Layers at high elevations, in the upper sections of the deposits, generally dipped away from the crater walls, along the direction of the wall slope. However, layers in several locations dip toward the crater wall. Fold structures in various locations in both Sera and Jiji are visible (Figure 10). An anticline was observed in Sera (Figures 10a and 10b) with layers dipping in excess of 22–40° in the fold limbs. The fold hinge is exposed revealing interior layering within the core (Figure 10). Three synclines and one anticline were observed in Jiji (Figure 11). Axial traces of the five folds trend 296–338° (i.e., general NW trend) and were determined by plotting poles of the layer attitudes into Schmidt-nets (example Figure 10d). Axial traces were then placed on the HRSC DEM to observe the regional pattern (Figure 11). In many cases, mounds themselves are made of folded beds (Figure 10c).

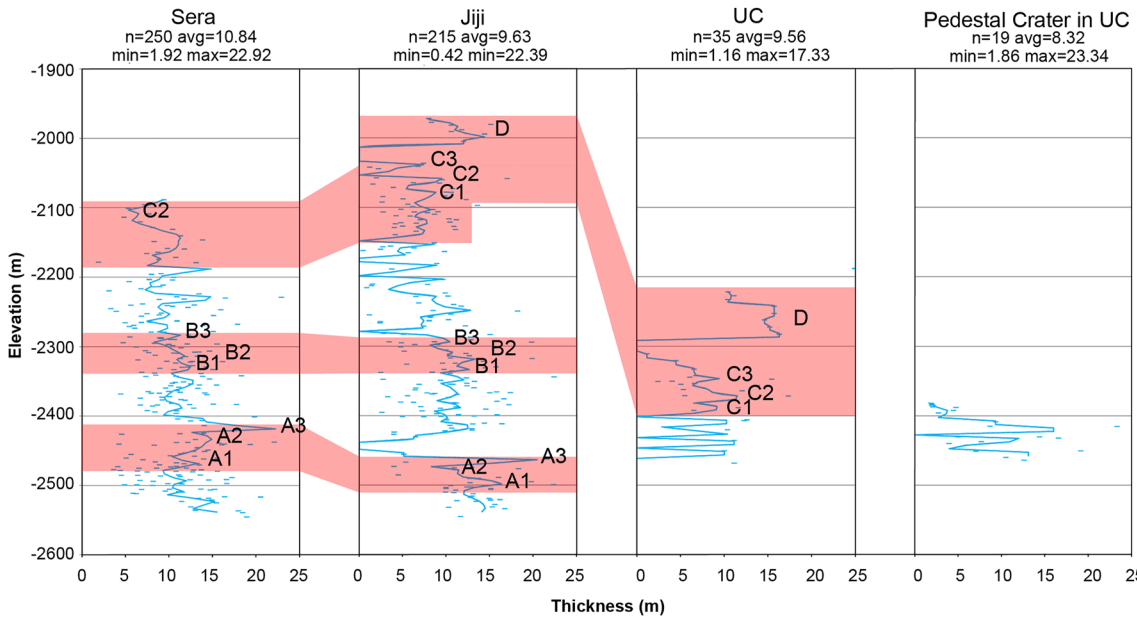

Figure 8. Layer thickness versus elevation graphs. Four main sequences have been identified: a lower sequence "A" (≈150 m thick), a middle sequence "B" (≈200 m thick), an upper sequence "C" (≈100–120 m thick), and a final sequence "D" (≈50 thick). Shaded red areas represent areas of correlation between craters. Peak thicknesses are labeled accordingly. Blue line represents average layer thickness in 10 m elevation intervals. Blue dashes represent individual measurements. The average thickness of layers correlated across craters are labeled A1–A3, B1–B3, C1–C3, and D. Sera, Jiji, and unnamed crater (UC) Pedestal Crater measured in 1 m/pixel High Resolution Imaging Science Experiment DEMs. UC is measured in a 10 m/pixel CTX digital elevation model (Table S1 in Supporting Information S1). Transects locations of layer measurements are available in Figure S2 of Supporting Information S1.

5. Discussion

5.1. Implications of Hydrated Sulfates Formation

The observed mineralogy has several implications for the genesis and/or alteration of the LD. Hydrous signatures were first observed 75 km northeast of the study area (Carter et al., 2013), as well as 250 km south of the mapping

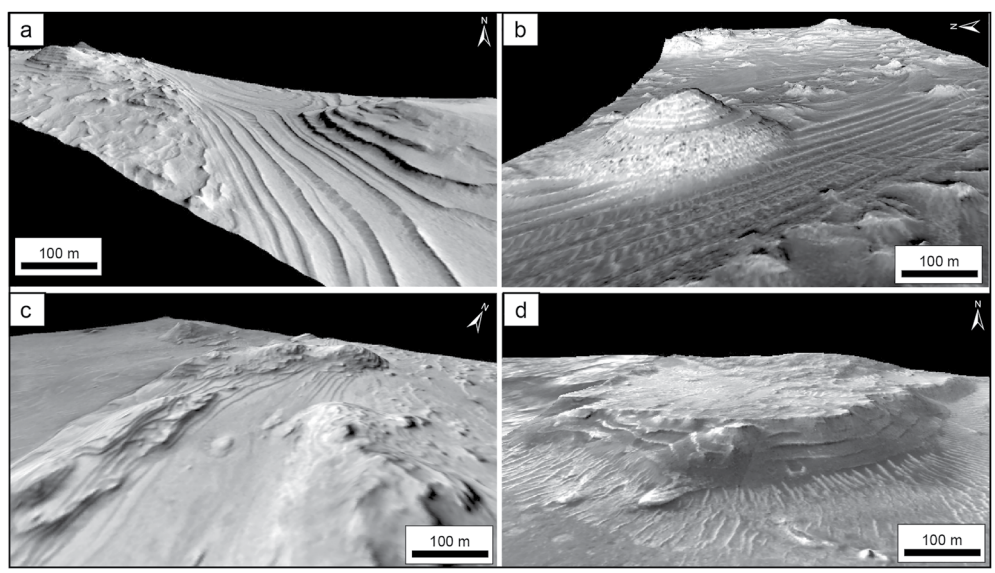

Figure 9. 3D view of sample layering from each crater and used image types in bracket. Regional figure locations are marked in Supporting Information S1. (a) Sera (High Resolution Imaging Science Experiment (HiRISE) n° ESP_057456_1890). (b) Jiji (HiRISE n° ESP_017013_1890). (c) Unnamed crater (UC) (CTX n° P15_006860_1902). (d) UC Pedestal Crater (HiRISE n° ESP_018714_1890).

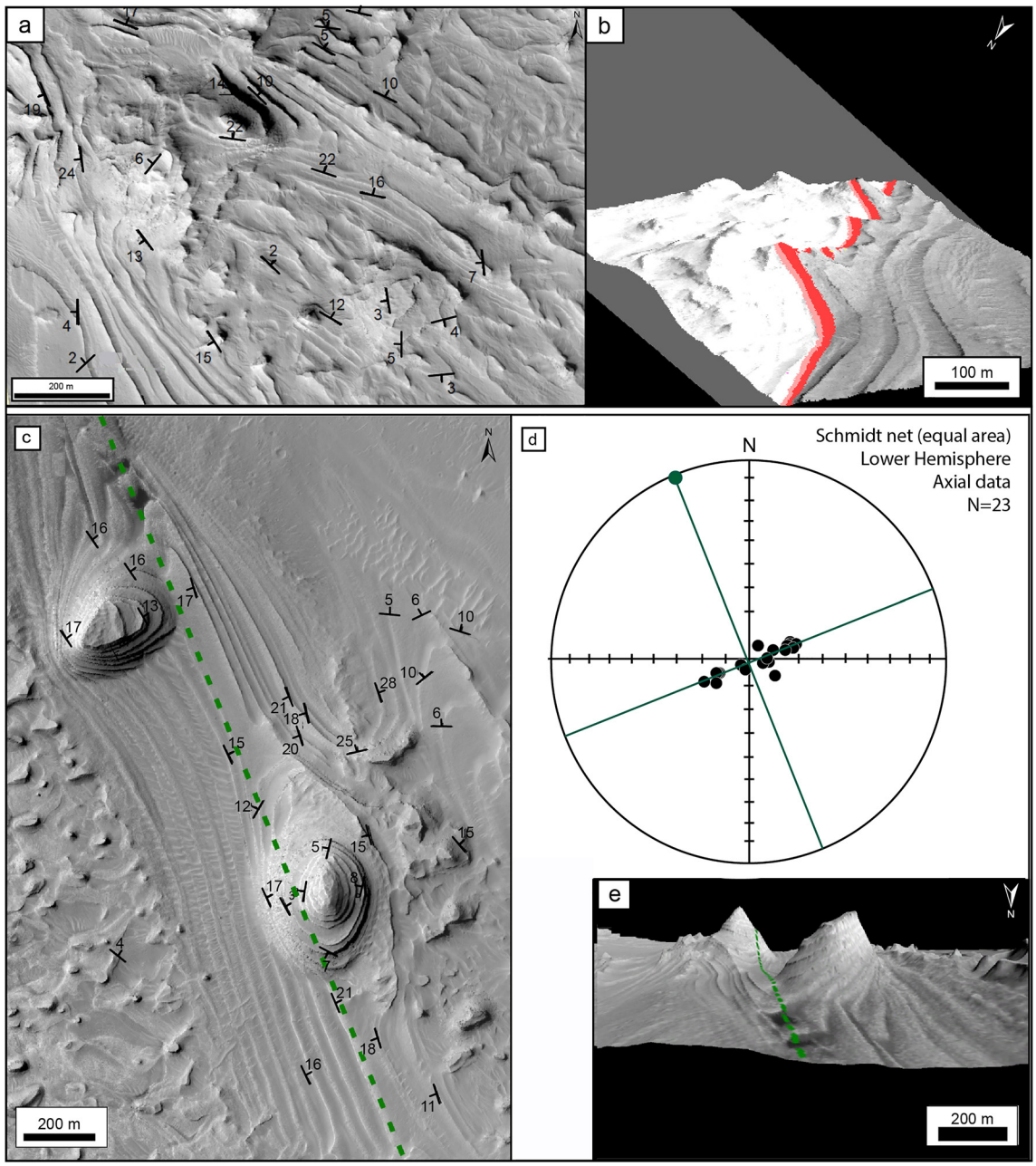

Figure 10. Anticline observed in Sera (a) Fold limbs dip southwest and northeast. The fold hinge has been eroded (High Resolution Imaging Science Experiment (HiRISE) n° ESP_057456_1890). (b) 3D example of high dips (30°+) within the southern limb. Figure S3 in Supporting Information S1 shows a panoramic view of panel (b). Structural analysis of a syncline observed in Jiji. (c) A syncline with layers in each limb dipping up to 21° (HiRISE n° ESP_017013_1890). Green line marks the axial trace trend. (d) Equal area Schmidt-net of the syncline showing an axial trend of 338°. (e) 3D view looking south down the axial trace that shows layers on either side dipping toward the fold axis (HiRISE n° ESP_017013_1890).

area in Meridiani Planum (Flahaut et al., 2015). Here, we observed spectral signatures typical of hydrated sulfates in agreement with Koeppel et al. (2022). We further observed different levels of sulfate hydration based on differences in the spectral signatures in our ROIs (Figure 6) which might be an indication of both monohydrated (i.e., kieserite) and polyhydrated (i.e., epsomite) sulfates. Monohydrated sulfates match well with the signature type found at lowest elevations (<−2,450 m) (Figure 6c) which mostly correspond to sequence A. We suggest kieserite due to its already established association with LD (Al-Samir et al., 2017; Fueten et al., 2014; Schmidt et al., 2018). On the other hand, the second signature type that might be related to the polyhydrated sulfate, that is, epsomite, was found only at higher elevations (>−2,400) corresponding to sequence B (Figure 6c).

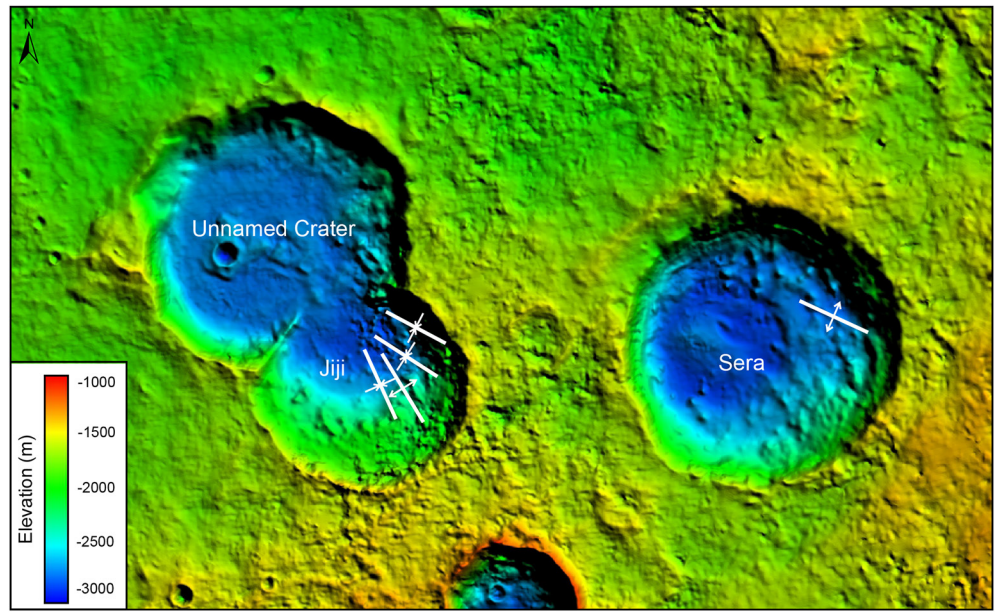

Figure 11. Observed folds within the layered deposits all trending NW–SE. Three synclines and one anticline in Jiji and one anticline observed in Sera. Background is MOLA over a hillshade background.

Several geochemical lab models show processes of dehydration from epsomite to kieserite due to different conditions such as humidity, temperature and pH (Al-Samir et al., 2017; Freeman et al., 2007; Gendrin et al., 2005; Noel et al., 2015). Specifically, epsomite precipitates during cooling of aqueous solution (Noel et al., 2015; Vaniman et al., 2004), whereas kieserite precipitates with increasing temperatures due to its negative temperature coefficient (Noel et al., 2015; Vaniman et al., 2004). The formation of kieserite heavily depends on temperature and humidity. Once formed however, it tends to persist over changes of temperature and relative humidity (Chipera & Vaniman, 2007). Specifically, kieserite can precipitate in environments with low pH (i.e., acidic environmental conditions) and higher temperature (ranged from 75 to 200°C) (Noel et al., 2015; Wang et al., 2009). Although the quality of the available spectra data cannot fully resolve a distinct boundary between mono- and polydrated sulfates and considering the different elevations where we observed monohydrated and polyhydrated sulfates, we can speculate about a mineralogical transition that may exist within our study area as a subsequent process of dehydration driven by diagenetic processes.

This type of transition has been observed previously in the LD within Valles Marineris, as well as Gale Crater (Flahaut et al., 2010; Fueten et al., 2014, 2017; Quantin et al., 2005; Schmidt et al., 2018). In Valles Marineris, this transition occurs over about 100 m of elevation (Flahaut et al., 2010; Schmidt et al., 2018), which is similar to what is observed in Sera. The difference in mineralogy could indicate compositional differences in the

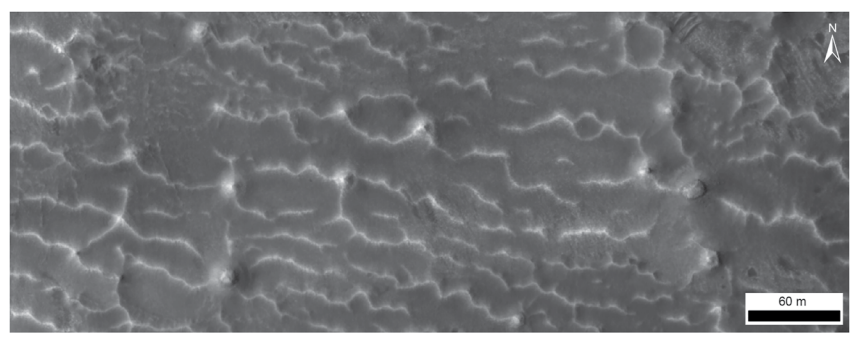

Figure 12. Zoomed view of Figure 6d (High Resolution Imaging Science Experiment image PSP_001902_1890) showing small mounds and fossil megaripples (MF) superposed on Equatorial Layered Deposits and associated with monohydrated sulfate detections (green dots in Figure 6d) in Compact Reconnaissance Imaging Spectrometer for Mars n. FRT000037F7.

sediment deposited at different elevations, or the temperature and composition of the water which permeated and cemented them. Alternatively, the dehydration of the polyhydrated sulfates only affected lower elevations (Al-Samir et al., 2017; Freeman et al., 2007; Gendrin et al., 2005; Mangold et al., 2008; Noel et al., 2015). Sulfur could have been brought by groundwater or would have already been present if the LD come from aeolian material eroded and reworked from volcanic deposits (Fueten et al., 2011, 2014; Le Deit et al., 2013; Schmidt et al., 2018). In the case of water, there could have initially been a particular composition and temperature which influenced the entire deposit, followed by a later event to −2,450 m of different temperature and composition. In Valles Marineris, it has been proposed that during a lake or standing water scenario, magmatic activity related to Tharsis was a heat source underneath the chasmata that raised the temperature needed for magnesium-hydrated sulfates to form (Al-Samir et al., 2017). However, no surficial evidence suggests a subterranean network of magmatic activity in Arabia Terra and thus it contrasts with the situation that could have occurred at the same time in Valles Marineris (Andrews-Hanna, 2012).

Independently from the source of the sulfur, water could have entered the crater through flooding, rain, groundwater recharge, or as percolating melted ice in a periglacial environment. However, since neither fluvial features, in plan view (e.g., Salese, Di Achille, et al., 2016) and in cross-section (e.g., Salese, McMahon, et al., 2020), nor obvious periglacial morphologies were observed entering or within the craters, groundwater is more likely source as previously suggested for other locations in Arabia Terra (Andrews-Hanna & Lewis, 2011; Andrews-Hanna et al., 2007, 2010; Franchi et al., 2014; Oehler & Allen, 2010; Pondrelli et al., 2015; Rossi et al., 2008; Zabrusky et al., 2012).

5.2. Implications of Layer Stratigraphy

Depositional conditions (i.e., energy) appear to have remained relatively constant throughout ELD deposition; however, thinning and thickening sequences do indicate small variations (Figure 8). The slightly smaller layer thickness range of Sera might indicate that more stable conditions were present than in Jiji. The overall trend from ≈15 m thick beds in the lower sequence "A" to ≈9 m thick beds in the upper sequence "C" might indicate a gradual shift to lower depositional energy throughout the entire deposition. The layers with thicknesses of 30–40 m between sequence "A" and "B" and sequence "B" and "C" that are present in Jiji and not present in Sera might indicate a lag in deposition and/or reflect the lower depositional energy of Sera.

The average layer thickness decreases 1.3 m from east/southeast to west/northwest across the study area. Sera (avg. 10.84 m) contains a slightly tighter range of thicknesses (1.92–22.92 m), whereas Jiji (avg. 9.63 m, range 0.42–22.39 m) contains thinner layers. The layer thickness average continues to decrease in UC (avg. 9.50) with a range of 1.16–17.33 m. This suggests an east-southeast to west-northwest trend that could represent a proximal-distal relationship to a source located in the east-southeast or differences in base levels between Sera and Jiji. In opposition to the decrease in layer thicknesses, Jiji contains an extra 110 m of ELDs at the uppermost elevations, which Sera does not. This contradicts a proximal-distal scenario unless there was an opposite erosional intensity trend which eroded Sera slightly more. Observable layering begins at the same ≈2,550 m elevation, so the added 110 m thickness of the ELDs in Jiji is likely not a product of differing crater depths at the onset of deposition. Since the thinning and thickening sequences are not an exact match between Sera and Jiji in both elevation and duration, we suggest that differences in a continuously fluctuating water level between the craters are a more attractive explanation. Based on elevation differences between the sequences, water-levels may have been 50–100 m different between the craters.

The observed folds could have formed syn-depositionally or post-depositionally. Since the NW–SE trend of the axial trace of each fold is found in both Sera and Jiji (Figure 11), they could be expressions of buried structures (Schmidt et al., 2018) such as a fault system that propagated through both craters prior to deposition. No major faulting was observed in layers of any fold limbs, which would indicate fault movement post-deposition. Lack of faults might mean compaction processes occurred. In a syn-depositional scenario, we can rule out deposition over a secondary crater ring, otherwise the axes would trend parallel to the crater wall. Draping over a preexisting topography with several layer attitudes exceeding 30° might be over the threshold for a layer to retain its bedding integrity; however, in compaction processes or if the sediment had enough cohesive strength, such dips could potentially be achieved. The fact that the observed fold axes in Jiji and Sera trend in an identical direction (NW–SE) may indicate a shared tectonic regime between the two craters which existed prior to deposition. Furthermore, the relationship between sedimentation rate, vertical displacement in the crater floor, and the duration of

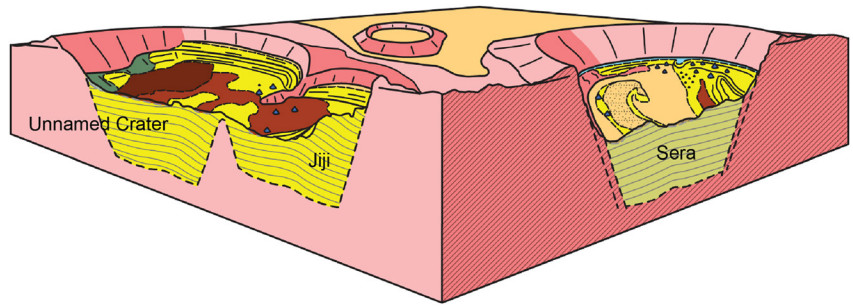

Figure 13. 3D view built starting from cross section X-X′ in Figure 2. Colors are the same as the map shown in Figure 2, although the lack of the gray-coded High-Resolution Stereo Camera mosaic below the sketch may result in some slight variations.

deposition might provide clues to the overall duration of the ELD formation by modeling layer compaction over fault scarps to determine what parameters achieve the observed layer attitudes.

5.3. Proposed Geological History

Based upon the current depositional architecture sketched in Figure 13 and mineralogical composition, together with results of previous studies, we propose the following scenario for the evolution of the study area. During the Early Noachian Epoch, the Arabia Terra region was extensively affected by large impact processes (Chapman & Jones, 1977) resulting in the formation of the oldest preserved crust in the region (unit B). Impact size and frequency generally decreased throughout the Noachian (Hartmann & Neukum, 2001) and moderately sized impacts generated craters like Sera and Jiji.

The unconformable deposition of LD in our study area generally occurred later than the cessation of the regional Late Noachian to Early Hesperian hydrological activity (Andrews-Hanna et al., 2010) and reflects a geological process active throughout Arabia Terra. Therefore, any formational hypothesis should explain a large-scale depositional process that operated in the region upon pre-existing topography and depositing layered sequences with thicknesses up to hundreds of meters associated with hydrous signatures.

Consistent with prior studies, observations have allowed the exclusion of some formation hypotheses from further consideration since no fluvial or deltaic or groundwater sapping evidence was found inside the study area (Davis et al., 2016; Lewis et al., 2008). Mud volcanoes and spring-mounds were also discounted as the origin of LM because no apical pits or breccia were recognized at the top of LM in the study area (Pondrelli et al., 2011).

Aeolian airfall or volcanic (i.e., pyroclastic) deposition might fit well in this context according to previous literature (Annex & Lewis, 2020; Hynek & Phillips, 2008; Koeppel et al., 2022; Schmidt et al., 2021; Zabrusky et al., 2012). For example, pyroclastic processes can occur over large distances and produce well-bedded deposits (Kerber et al., 2013; Rose et al., 2003) providing an explanation for the widespread presence and the repetitive horizontal to sub-horizontal layering of ELDs in the region. On the other hand, non-pyroclastic airfall is consistent with the expected time scales of formation (Lewis & Aharonson, 2014) and current dust accumulation rates on Mars (Annex & Lewis, 2020; Johnson et al., 2003), as it has previously been suggested for LD elsewhere in Arabia Terra (Bridges & Muhs, 2012; Fergason & Christensen, 2008; Koeppel et al., 2022; Squyres & Knoll, 2005). The Loess Plateau, China, would be a plausible "dry" terrestrial analog for the well-bedded air-fall deposits in the study area (Pye, 1995; Verosub et al., 1993) due to the possible draping, horizontal extent, highly repetitive layering, and erodibility (Fu et al., 2000). Annex & Lewis, 2020, observed a comparable trend in Sera and Jiji as well as in several other craters in Arabia Terra, concluding that a similar aeolian depositional process might resemble the one that emplaced the proposed Earth analog.

However, mere aeolian environments have several controlling mechanisms (i.e., wind patterns, pressure gradients, and topography) (Kocurek, 1988) leading to stochastic (i.e., random) packaging (Cadieux & Kah, 2015). Furthermore, it has also been considered that tectonic subsidence (and/or uplift) played little to no role in controlling the accommodation space in the study area since the region of Arabia Terra is considered tectonically inactive at the time of deposition and since (Barlow, 2008). In agreement with the layer thickness measurements presented by

Annex and Lewis (2020), the occurrence of trending thinning and thickening sequences outlined non-stochastic stacking patterns. This makes airfall deposition—in the absence of a layer thickness control (e.g., climate cycles as proposed by Lewis and Aharonson (2014)) or a regional aqueous base level as proposed by Cadieux and Kah (2015)—an improbable model to describe the layered succession deposited in Sera and Jiji. In the absence of random (i.e., stochastic) stratal patterns, tectonics and fluvial evidence, we suggest the occurrence of trending sequences (whether thinning or thickening) and hydrated minerals resulting from an aeolian depositional environment with sediment accumulation primarily driven by the fluctuation of an air-water interface within a groundwater reservoir like the one proposed for Meridiani Planum (Andrews-Hanna et al., 2007, 2010). This aquifer can be assumed to be confined with a non-uniform rising of water through faults and/or fractures, commonly present and distributed over the area. Therefore, a locally different groundwater table rise in a playa-like environment could have led to different rates of cementation and, consequently, of preservation potential of aeolian sands and associated bedforms. Nevertheless, global hydrological models of a precipitation-evaporation-driven hydrological cycle also confirm that the Arabia Terra region (and Meridiani Planum) is a preferred site for groundwater upwelling, driven primarily by the distinctive topography of Arabia Terra (Andrews-Hanna et al., 2007). This scenario is also bolstered by previous mineralogical results (e.g., Zabrusky et al., 2012), which point to a fluctuating groundwater table in an acidic environment which subjects bedrock, composed of clinopyroxene (augite), and olivine (forsterite) to chemical alteration under special circumstances (Marcucci & Hynek, 2014; McCollom et al., 2013). An intermittent water presence in this area has also been proposed by Koeppel et al. (2022), though they propose that based on low cohesion of the sediment, the origin of the ELD is related to dust accumulation indurated with sulfate precipitation requiring a minimal amount of water. However, unknown details of the ELD's grain sorting, as well as the degree to which thermal inertia can be influenced by dust deposition and wind, make it unresolved to determine the intensity and volume of water present in the craters during deposition. In our scenario, the hydrated mineral formation represents the late stages of water activity, where an evaporative environment became dominant.

Although, the extent to which water contributed to LD is still debated between persistent, water-stable (Andrews-Hanna et al., 2010; Pondrelli et al., 2019; Wiseman et al., 2010; Zabrusky et al., 2012) or intermittent conditions (Koeppel et al., 2022). Isolated impact-induced greenhouse climates (Segura et al., 2002) or localized volcanic warming of the subsurface (McCollom & Hynek, 2005) is not spatially and temporally congruous with the regional nature of the hydrological cycle represented in Arabia Terra. However, a planet-wide groundwater system on Mars has been previously proposed in order to explain evidence of fluvio-lacustrine environments in deep crater basins (<−4,000 m) (Salese et al., 2019). In this light, it might be hypothesized that this groundwater system also affects, possibly due to peculiar local subsurface settings (e.g., tectonics, dikes), shallower basins such as Sera and Jiji (>−3,500 m) to a lesser extent. The importance of groundwater to control LD formation/preservation under an aeolian regime has been previously proposed within both a warm Martian climate (Andrews-Hanna & Lewis, 2011; Andrews-Hanna et al., 2010) and a cold, early Mars with a predominantly frozen groundwater reservoir (Fairén, 2010; Kite, Halevy, et al., 2013). Previous interpretations of astronomical forcing of sedimentary packages (Lewis et al., 2008) are consistent with both climatic regimes since evidence highlights that both liquid and ice water have been present on or near the surface through the planet's history (Andrews-Hanna et al., 2010; Bibring et al., 2005; Fastook et al., 2008; Parker et al., 1993; Poulet et al., 2005; Squyres & Knoll, 2005).

Eventually, the analysis of orbital observations outlined evidence of a complex depositional environment where several geological processes coexisted and interacted. We also favor a multiple stage history of sulfate formation that may have differed in duration and/or water chemistry, where the key differences were in the environment rather than the composition of the deposits themselves. Regardless of whichever process or environmental conditions that emplaced LD, the detection of hydrated sulfates in correspondence of both LD (Figure 6) and small mounds and fossil megaripples (Figure 6d) further testifies how crucial a near-surface regional-scale aquifer is, not only as a controlling factor for layer trends but also for the cementation and preservation of LD, LM, and MF. If HiRISE observations reveal that LD and LM are a locally variable morphological expression of the same lithology (i.e., texturally indistinguishable), mineralogical results reveal that LD and fossil megaripples are genetically correlated: megaripples derive from the erosion, reworking and redeposition of the LD. Furthermore, megaripples are usually not preserved in the geological record, but the induration caused by groundwater allowed the preservation of these bedforms, which point to a relatively constant wind regime through the geological time considering the current one (≈NE–SW). This preservation coupled with the non-stochastic pattern of ELDs leads

to speculation about a more geologically stable water table and consequent induration, rather than an episodic one as proposed by Koeppel et al. (2022). A fluctuating aquifer throughout the crater's history may also explain elevation trends of unit *T*, which might have been favored by the distribution of fractures along the crater rim. However, it is unrealistic to define this topographic relation with just two craters which differ greatly in areal extent and lack an observable rim. Retrieving and analyzing such values over a significant number of craters/basins would help to constrain a possible relation between groundwater rise, topography, and fracture distribution. Eventually, it must be considered that the extent of this unit is very limited (especially in Jiji) and it is also heavily affected by erosion. Therefore, any other speculation requires further and more focused analyses.

In the most recent history of the study area, different coverages, and generations of AD have formed. Present activity is dominated by wind erosion, which is currently developing barchan dunes and accumulating loose material (AD, Figures 3b, 5c, and 5d) under the current and relatively uniform wind system (≈NE–SW) (Cardinale et al., 2020; Silvestro et al., 2021). Recent megaripples and dark dunes are just the most recent indicators of a long history of erosion and deposition attesting to the ongoing wind activity. To decipher what led to the transition to one generation from the other, and the timing, is an interesting perspective that remains open.

6. Conclusion

The ELDs that widely outcrop throughout Mars' low latitudes have long been an enigma in uncovering past climatic conditions of Mars. Although the role and duration of water in their formation is still debated, these deposits contain unique records of aqueous conditions and reflect a sedimentological response to variations in depositional processes, pointing to a combination of sediment input, base level and accommodation space changes. We outlined evidence of a complex depositional environment where several geological processes coexisted and interacted. Using stratigraphy, bedding orientation and layer thickness, we were able to reconstruct the geological history within the study area by comparing LD. The analysis and correlation of the stratigraphic sequences in the basins tested the presence of common trends and led us to infer the nature of the controls on deposition. Layered deposits within Sera and Jiji preserve an exceptional record of past climatic conditions of the Arabia Terra region. Due to the thinning and thickening sequences identified from layer thickness measurements, mere subaerial deposition hypotheses (i.e., airfall deposition, volcanic or impact related ejecta) with no aqueous component is unlikely. We concluded that LD are deposited in an aeolian environment controlled by a changing base-level of a near-surface aquifer. The variations observed in layering sequences likely reflect a significant control by groundwater-level fluctuations during deposition. The proposed long-term water level combined with the regional layer thickness trend does help support the idea that water level influences layer formation. The lack of any apparent fluvial or lacustrine features flowing into or within Sera and Jiji does not link the LD to surficial water-related sediment transport and led us to discard these hypotheses from further consideration for the aqueous input. Our work shows that the same ELDs unit fills both Sera and Jiji and likely had a larger extent over the map region (and in Arabia Terra), possibly because syndepositional settings (and locally groundwater upwelling) contributed to enhanced cementation in these locales and/or they are more protected from deflation. In fact, observed layered morphologies, LD and mounds, result from differential cementation of a single lithology since lateral continuity and no other difference in texture or pattern was observed. Eventually, this differential erosion can result from many factors including local and regional differences in wind speed through time, and differences in the mechanical properties as well as the degree of cementation of the deposits.

Independently from the discrete depositional process or conditions which emplaced the LD, the observed hydrous signatures further reinforce the interaction of an aqueous component that possibly altered and cemented the LD in the study area. Evidence of multiple sulfate-rich deposits have been observed leading to the possibility of different formation environments which are useful for understanding the acidic paleo-environmental conditions and evolution of an area. Nevertheless, according to the stratigraphic distribution (Noachian-Hesperian transition up to the lower Hesperian) and our mineralogical observation, ELDs in Sera and Jiji would postdate the clay-bearing deposits of Noachian age, and thus confirm the increasing to a stronger acidic environment in the Hesperian period in Mars history.

Such complex depositional scenarios cannot be deciphered by the analysis of solely three target craters, but rather scientific outcomes would exponentially be increased by broadening the population of small basins where detailed analyses of ELDs are performed. Retrieving and analyzing layering over a significant number of craters/basins has helped to show a general SE–NW decrease in layer thicknesses from our study area to the northwestern

edge of Arabia Terra; however, the absence of ELDs within craters/basins of similar topographic relations and dimensions as those with the presence of ELDs remains poorly understood. Finally, forthcoming works should address open questions, further investigating and unraveling the nature of LD since they are globally significant paleoclimatic archive of Mars' history and its potential habitability conditions.

Data Availability Statement

We used data reposited into the PDS Geosciences Node in the creation of this manuscript. References to the datasets mentioned in the methodology section are CTX (Malin, 2007), HiRISE (McEwen, 2007), MOLA data (Smith, 1999), CRISM (Murchie, 2006), and THEMIS (Christensen et al., 2004). This research has also made use of the USGS ISIS (https://isis.astrogeology.usgs.gov/Installation/index.html) to radiometrically correct and project CTX and HiRISE images, which in turn were then processed to produce Digital Elevation Models through the NASA Ames Stereo Pipeline (https://ti.arc.nasa.gov/tech/asr/groups/intelligent-robotics/ngt/stereo/#Downloading). The processing of spectral data used the Image Processing & Analysis Software ENVI® (https://www.l3harrisgeospatial.com/Software-Technology/ENVI), the Analysis Tool CAT 7.4 developed for the ENVI© software available at https://pds-geosciences.wustl.edu/missions/mro/crism.htm and the RELAB () and USGS (https://crustal.usgs.gov/speclab/data/HTMLmetadata/README/splib07_DataSeries.htm). We also used the Orion software (Pangaea Scientific, 2006) and plotted on Schmidt-nets for layering observations.

Acknowledgments
This work was co-funded by the In-Time project (G.A. 823934) and Europlanet GMAP (G.A. 871149) within the Horizon 2020 programme of the European Union. F. Salese and A. G. Fairén are supported by "MarsFirstWater," funded by the European Research Council, Consolidator Grant 818602. A special thanks goes to Dr. Ettore Perozzi (Italian Space Agency, Italy) who made it possible to conclude the study.

References

Allen, C. C., & Oehler, D. Z. (2008). A case for ancient springs in Arabia Terra, Mars. *Astrobiology*, *8*(6), 1093–1112. https://doi.org/10.1089/ast.2008.0239

Al-Samir, M., Nabhan, S., Fritz, J., Winkler, A., Bishop, J. L., Gross, C., & Jaumann, R. (2017). The paleolacustrine evolution of Juventae Chasma and Maja Valles and its implications for the formation of interior layered deposits on Mars. *Icarus*, *292*, 125–143. https://doi.org/10.1016/j.icarus.2016.12.023

Andrews-Hanna, J. C. (2012). The formation of Valles Marineris: 3. Trough formation through super-isostasy, stress, sedimentation, and subsidence. *Journal of Geophysical Research*, *117*(E6), E06002. https://doi.org/10.1029/2012je004059

Andrews-Hanna, J. C., & Lewis, K. W. (2011). Early Mars hydrology: 2. Hydrological evolution in the Noachian and Hesperian epochs. *Journal of Geophysical Research*, *116*(E2), E02007. https://doi.org/10.1029/2010je003709

Andrews-Hanna, J. C., Phillips, R. J., & Zuber, M. T. (2007). Meridiani Planum and the global hydrology of Mars. *Nature*, *446*(7132), 163–166. https://doi.org/10.1038/nature05594

Andrews-Hanna, J. C., Zuber, M. T., Arvidson, R. E., & Wiseman, S. M. (2010). Early Mars hydrology: Meridiani playa deposits and the sedimentary record of Arabia Terra. *Journal of Geophysical Research*, *115*(E6), E06002. https://doi.org/10.1029/2009je003485

Andrews-Hanna, J. C., Zuber, M. T., & Banerdt, W. B. (2008). The Borealis basin and the origin of the martian crustal dichotomy. *Nature*, *453*(7199), 1212–1215. https://doi.org/10.1038/nature07011

Annex, A. M., & Lewis, K. W. (2020). Regional correlations in the layered deposits of Arabia Terra, Mars. *Journal of Geophysical Research: Planets*, *125*(6), e2019JE006188. https://doi.org/10.1029/2019JE006188

Ansan, V., Loizeau, D., Mangold, N., Le Mouélic, S., Carter, J., Poulet, F., et al. (2011). Stratigraphy, mineralogy, and origin of layered deposits inside Terby crater, Mars. *Icarus*, *211*(1), 273–304. https://doi.org/10.1016/j.icarus.2010.09.011

Baioni, D., & Tramontana, M. (2017). Possible evaporite karst in an interior layered deposit in Juventae Chasma, Mars. *International Journal of Speleology*, *46*(2), 181–189. https://doi.org/10.5038/1827-806X.46.2.2085

Balme, M., Berman, D. C., Bourke, M. C., & Zimbelman, J. R. (2008). Transverse aeolian ridges (TARs) on Mars. *Geomorphology*, *101*(4), 703–720. https://doi.org/10.1016/j.geomorph.2008.03.011

Balme, M. R., Gupta, S., Davis, J. M., Fawdon, P., Grindrod, P. M., Bridges, J. C., et al. (2020). Aram Dorsum: An extensive mid-Noachian age fluvial depositional system in Arabia Terra, Mars. *Journal of Geophysical Research: Planets*, *125*(5), e2019JE006244. https://doi.org/10.1029/2019je006244

Bargar, K. E. (1978). *Geology and thermal history of Mammoth Hot Springs, Yellowstone National Park, Wyoming (No. USGS-BULL-1444)*. Wyoming Geological Survey.

Barlow, N. (2008). *Mars: An introduction to its interior, surface and atmosphere* (Vol. 163). Cambridge University Press.

Bernhardt, H., Hiesinger, H., Ivanov, M. A., Ruesch, O., Erkeling, G., & Reiss, D. (2016). Photogeologic mapping and the geologic history of the Hellas basin floor, Mars. *Icarus*, *264*, 407–442. https://doi.org/10.1016/j.icarus.2015.09.031

Bibring, J. P., Langevin, Y., Gendrin, A., Gondet, B., Poulet, F., Berthé, M., et al. (2005). Mars surface diversity as revealed by the OMEGA/Mars Express observations. *Science*, *307*(5715), 1576–1581. https://doi.org/10.1126/science.1108806

Bibring, J. P., Langevin, Y., Mustard, J. F., Poulet, F., Arvidson, R., Gendrin, A., et al. (2006). Global mineralogical and aqueous Mars history derived from OMEGA/Mars Express data. *Science*, *312*(5772), 400–404. https://doi.org/10.1126/science.1122659

Bishop, J. L., Parente, M., Wietz, C. M., Noe Dobrea, E. Z., Roach, L. H., Murchie, S. L., et al. (2009). Mineralogy of Juventae Chasma: Sulfates in the light-toned mounds, mafic minerals in the bedrock, and hydrated silica and hydroxylatedferric sulfate on the plateau. *Journal Geophysical Research*, *114*, E00D09. https://doi.org/10.1029/2009je003352

Bridges, N. T., & Muhs, D. R. (2012). Duststones on Mars: Source, transport, deposition, and erosion. *Sedimentary geology of Mars*, *102*, 169–182.

Broxton, M. J., & Edwards, L. J. (2008). The Ames Stereo Pipeline: Automated 3D surface reconstruction from orbital imagery. In *Paper presented at 39th Annual Lunar and Planetary Science Conference* (Vol. 1391, p. 2419).

Cadieux, S. B., & Kah, L. C. (2015). To what extent can intracrater layered deposits that lack clear sedimentary textures be used to infer depositional environments? *Icarus*, *248*, 526–538. https://doi.org/10.1016/j.icarus.2014.11.004

Cardinale, M., Pozzobon, R., Tangari, A. C., Runyon, K., Di Primio, M., & Marinangeli, L. (2020). Reconstruction of the sand transport pathways and provenance in Moreux crater, Mars. *Planetary and Space Science*, *181*, 104788. https://doi.org/10.1016/j.pss.2019.104788

Carter, J., Poulet, F., Bibring, J. P., Mangold, N., & Murchie, S. (2013). Hydrous minerals on Mars as seen by the CRISM and OMEGA imaging spectrometers: Updated global view. *Journal of Geophysical Research: Planets*, *118*(4), 831–858. https://doi.org/10.1029/2012je004145

Chapman, C. R., & Jones, K. L. (1977). Cratering and obliteration history of Mars. *Annual Review of Earth and Planetary Sciences*, *5*(1), 515–538. https://doi.org/10.1146/annurev.ea.05.050177.002503

Chapman, M. G., & Tanaka, K. L. (2002). Related magma–ice interactions: Possible origins of chasmata, chaos, and surface materials in Xanthe, Margaritifer, and Meridiani Terrae, Mars. *Icarus*, *155*(2), 324–339. https://doi.org/10.1006/icar.2001.6735

Chipera, S. J., & Vaniman, D. T. (2007). Experimental stability of magnesium sulfate hydrates that may be present on Mars. *Geochimica et Cosmochimica Acta*, *71*(1), 241–250. https://doi.org/10.1016/j.gca.2006.07.044

Christensen, P. R., Jakosky, B. M., Kieffer, H. H., Malin, M. C., McSween, H. Y., Nealson, K., et al. (2004). The thermal emission imaging system (THEMIS) for the Mars 2001 Odyssey Mission. *Space Science Reviews*, *110*(1–2), 85–130. https://doi.org/10.1023/b:spac.0000021008.16305.94

Christie-Blick, N., & Driscoll, N. W. (1995). Sequence stratigraphy. *Annual Review of Earth and Planetary Sciences*, *23*(1), 451–478. https://doi.org/10.1146/annurev.ea.23.050195.002315

Chukanov, N. V. (2014). IR spectra of minerals and reference samples data. In *Infrared spectra of mineral species* (pp. 21–1701). Springer.

Clark, R. N., King, T. V., Klejwa, M., Swayze, G. A., & Vergo, N. (1990). High spectral resolution reflectance spectroscopy of minerals. *Journal of Geophysical Research*, *95*(B8), 12653–12680. https://doi.org/10.1029/JB095iB08p12653

Davis, J. M., Balme, M., Grindrod, P. M., Williams, R. M. E., & Gupta, S. (2016). Extensive Noachian fluvial systems in Arabia Terra: Implications for early Martian climate. *Geology*, *44*(10), 847–850. https://doi.org/10.1130/g38247.1

Davis, J. M., Grindrod, P., Fawdon, P., Williams, R., Gupta, S., & Balme, M. (2018). Episodic and declining fluvial processes in southwest Melas Chasma, Valles Marineris, Mars. *Journal of Geophysical Research: Planets*, *123*(10), 2527–2549. https://doi.org/10.1029/2018JE005710

Davis, J. M., Gupta, S., Balme, M., Grindrod, P. M., Fawdon, P., Dickeson, Z. I., & Williams, R. M. (2019). A diverse array of fluvial depositional systems in Arabia Terra: Evidence for mid-Noachian to early Hesperian rivers on Mars. *Journal of Geophysical Research: Planets*, *124*(7), 1913–1934. https://doi.org/10.1029/2019je005976

Day, M., Anderson, W., Kocurek, G., & Mohrig, D. (2016). Carving intracrater layered deposits with wind on Mars. *Journal of Geophysical Research Letters*, *43*(6), 2473–2479. https://doi.org/10.1002/2016gl068011

Day, M. D., & Catling, D. C. (2020). Potential aeolian deposition of intra-crater layering: A case study of Henry crater, Mars. *GSA Bulletin*, *132*(3–4), 608–616. https://doi.org/10.1130/b35230.1

Di Pietro, I., Ori, G. G., Pondrelli, M., & Salese, F. (2018). Geology of Aeolis Dorsa alluvial sedimentary basin, Mars. *Journal of Maps*, *14*(2), 212–218. https://doi.org/10.1080/17445647.2018.1454350

Edgett, K. S., & Malin, M. C. (2002). Martian sedimentary rock stratigraphy: Outcrops and interbedded craters of northwest Sinus Meridiani and southwest Arabia Terra. *Journal of Geophysical Research Letters*, *29*(24), 32-1–32-4. https://doi.org/10.1029/2002GL016515

Fairén, A. G. (2010). A cold and wet Mars. *Icarus*, *208*(1), 165–175. https://doi.org/10.1016/j.icarus.2010.01.006

Fastook, J. L., Head, J. W., Merchant, D. R., & Forget, F. (2008). Tropical mountain glacier on Mars: Altitude dependence of ice accumulation, accumulation conditions, formation times, glacier dynamics, and implications for planetary spin-axis/orbital history. *Icarus*, *198*(2), 305–317. https://doi.org/10.1016/j.icarus.2008.08.008

Fergason, R. L., & Christensen, P. R. (2008). Formation and erosion of layered materials: Geologic and dust cycle history of eastern Arabia Terra, Mars. *Journal of Geophysical Research*, *113*(E12), E12001. https://doi.org/10.1029/2007je002973

Flahaut, J., Carter, J., Poulet, F., Bibring, J. P., Van Westrenen, W., Davies, G. R., & Murchie, S. L. (2015). Embedded clays and sulfates in Meridiani Planum, Mars. *Icarus*, *248*, 269–288. https://doi.org/10.1016/j.icarus.2014.10.046

Flahaut, J., Quantin, C., Allemand, P., Thomas, P., & Le Deit, L. (2010). Identification, distribution and possible origins of sulfates in Capri Chasma (Mars), inferred from CRISM data. *Journal of Geophysical Research*, *115*(E11), E11007. https://doi.org/10.1029/2009je003566

Franchi, F., Rossi, A. P., Pondrelli, M., & Cavalazzi, B. (2014). Geometry, stratigraphy and evidences for fluid expulsion within Crommelin crater deposits, Arabia Terra, Mars. *Planetary and Space Science*, *92*, 34–48. https://doi.org/10.1016/j.pss.2013.12.013

Freeman, J., Wang, A., & Jolliff, B. (2007). Pathways to form kieserite from epsomite at mid to low temperatures, with relevance to Mars. In *Paper presented at 38th Annual Lunar and Planetary Science Conference* (Vol. 1338, p. 1298).

Fu, B., Chen, L., Ma, K., Zhou, H., & Wang, J. (2000). The relationships between land use and soil conditions in the hilly area of the loess plateau in northern Shaanxi, China. *Catena*, *39*(1), 69–78. https://doi.org/10.1016/s0341-8162(99)00084-3

Fueten, F., Flahaut, J., Le Deit, L., Stesky, R., Hauber, E., & Gwinner, K. (2011). Interior layered deposits within a perched basin, southern Coprates Chasma, Mars: Evidence for their formation, alteration, and erosion. *Journal of Geophysical Research*, *116*(E2), E02003. https://doi.org/10.1029/2010je003695

Fueten, F., Flahaut, J., Stesky, R., Hauber, E., & Rossi, A. P. (2014). Stratigraphy and mineralogy of Candor Mensa, West Candor Chasma, Mars: Insights into the geologic history of Valles Marineris. *Journal of Geophysical Research: Planets*, *119*(2), 331–354. https://doi.org/10.1002/2013je004557

Fueten, F., Novakovic, N., Stesky, R., Flahaut, J., Hauber, E., & Rossi, A. P. (2017). The evolution of Juventae Chasma, Valles Marineris, Mars: Progressive Collapse and Sedimentation. *Journal of Geophysical Research: Planets*, *122*(11), 2223–2249. https://doi.org/10.1002/2017je005334

Fueten, F., Stesky, R., MacKinnon, P., Hauber, E., Zegers, T., Gwinner, K., et al. (2008). Stratigraphy and structure of interior layered deposits in west Candor Chasma, Mars, from High Resolution Stereo Camera (HRSC) stereo imagery and derived elevations. *Journal of Geophysical Research*, *113*(E10), E11004. https://doi.org/10.1029/2007JE003053

Garvin, J. B., Sakimoto, S. E. H., & Frawley, J. J. (2003). Craters on Mars: Global geometric properties from gridded MOLA. In *Paper presented at 6th International Conference on Mars* (Vol. 3).

Gendrin, A., Mangold, N., Bibring, J. P., Langevin, Y., Gondet, B., Poulet, F., et al. (2005). Sulfates in Martian layered terrains: The OMEGA/Mars Express view. *Science*, *307*(5715), 1587–1591. https://doi.org/10.1126/science.1109087

Glotch, T., & Rogers, A. (2007). Evidence for aqueous deposition of hematite- and sulfate-rich light-toned layered deposits in Aureum and Iani Chaos, Mars. *Journal of Geophysical Research*, *112*(E6), E06001. https://doi.org/10.1029/2006JE002863

Greeley, R., & Guest, J. (1987). *Geologic map of the eastern equatorial region of Mars*. Geological Survey.

Grotzinger, J., Beaty, D., Dromart, G., Gupta, S., Harris, M., Hurowitz, J., et al. (2011). Mars sedimentary geology: Key concepts and outstanding questions. *Astrobiology*, *11*(1), 77–87. https://doi.org/10.1089/ast.2010.0571

Grotzinger, J. P., Arvidson, R. E., Bell, J. F., III, Calvin, W., Clark, B. C., Fike, D. A., et al. (2005). Stratigraphy and sedimentology of a dry to wet aeolian depositional system, Burns formation, Meridiani Planum, Mars. *Earth and Planetary Science Letters*, *240*(1), 11–72. https://doi.org/10.1016/j.epsl.2005.09.039

Grotzinger, J. P., & Milliken, R. E. (2012). The sedimentary rock record of Mars: Distribution, origins, and global stratigraphy. *Sedimentary Geology of Mars*, *102*, 1–48.
Hartmann, W. K., & Neukum, G. (2001). Cratering chronology and the evolution of Mars. In *Chronology and evolution of Mars: Proceedings of an ISSI Workshop, 10–14 April 2000, Bern, Switzerland* (pp. 165–194). Springer.
Hugenholtz, C. H., Barchyn, T. E., & Boulding, A. (2017). Morphology of transverse aeolian ridges (TARs) on Mars from a large sample: Further evidence of a megaripple origin? *Icarus*, *2*, 193–201. https://doi.org/10.1016/j.icarus.2016.10.015
Hunt, G. R. (1970). Visible and near-infrared spectra of minerals and rocks: I silicate minerals. *Modern Geology*, *1*, 283–300.
Hurst, A., Scott, A., & Vigorito, M. (2011). Physical characteristics of sand injectites. *Earth-Science Reviews*, *106*(3–4), 215–246. https://doi.org/10.1016/j.earscirev.2011.02.004
Hynek, B. M., Arvidson, R. E., & Phillips, R. J. (2002). Geologic setting and origin of Terra Meridiani hematite deposit on Mars. *Journal of Geophysical Research*, *107*(E10), 18-1–18-14. https://doi.org/10.1029/2002je001891
Hynek, B. M., & Di Achille, G. (2017). *Geologic map of Meridiani Planum, Mars*. US Geological Survey Scientific Investigations Map (p. 3356).
Hynek, B. M., & Phillips, R. J. (2001). Evidence for extensive denudation of the Martian highlands. *Geology*, *29*(5), 407–410. https://doi.org/10.1130/0091-7613(2001)029<0407:efedot>2.0.co;2
Hynek, B. M., & Phillips, R. J. (2008). The stratigraphy of Meridiani Planum, Mars, and implications for the layered deposits' origin. *Earth and Planetary Science Letters*, *274*(1–2), 214–220. https://doi.org/10.1016/j.epsl.2008.07.025
Itok, Y., & Parente, M. A. (2021). New method for atmospheric correction and denoising CRISM hyperspectral data. *Icarus*, *345*, 114024.
Johnson, J. R., Grundy, W. M., & Lemmon, M. T. (2003). Dust deposition at the Mars Pathfinder landing site: Observations and modeling of visible/near-infrared spectra. *Icarus*, *163*(2), 330–346. https://doi.org/10.1016/s0019-1035(03)00084-8
Kerber, L., Forget, F., Madeleine, J. B., Wordsworth, R., Head, J. W., & Wilson, L. (2013). The effect of atmospheric pressure on the dispersal of pyroclasts from martian volcanoes. *Icarus*, *223*(1), 149–156. https://doi.org/10.1016/j.icarus.2012.11.037
Kerber, L., Head, J. W., Madeleine, J. B., Forget, F., & Wilson, L. (2012). The dispersal of pyroclasts from ancient explosive volcanoes on Mars: Implications for the friable layered deposits. *Icarus*, *219*(1), 358–381. https://doi.org/10.1016/j.icarus.2012.03.016
Kite, E. S. (2019). Geologic constraints on early Mars climate. *Space Science Reviews*, *215*(1), 1–47. https://doi.org/10.1007/s11214-018-0575-5
Kite, E. S., Halevy, I., Kahre, M. A., Wolff, M. J., & Manga, M. (2013). Seasonal melting and the formation of sedimentary rocks on Mars, with predictions for the Gale Crater mound. *Icarus*, *223*(1), 181–210. https://doi.org/10.1016/j.icarus.2012.11.034
Kite, E. S., Lewis, K. W., Lamb, M. P., Newman, C. E., & Richardson, M. I. (2013). Growth and form of the mound in Gale Crater, Mars: Slope wind enhanced erosion and transport. *Geology*, *41*(5), 543–546. https://doi.org/10.1130/g33909.1
Kite, E. S., & Mayer, D. P. (2017). Mars sedimentary rock erosion rates constrained using crater counts, with applications to organic-matter preservation and to the global dust cycle. *Icarus*, *286*, 212–222. https://doi.org/10.1016/j.icarus.2016.10.010
Klima, R. L., Pieters, C. M., & Dyar, M. D. (2007). Spectroscopy of synthetic Mg-Fe pyroxenes I: Spin-allowed and spin-forbidden crystal field bands in the visible and near-infrared. *Meteoritics and Planetary Science*, *42*(2), 235–253. https://doi.org/10.1111/j.1945-5100.2007.tb00230.x
Knauth, L. P., Burt, D. M., & Wohletz, K. H. (2005). Impact origin of sediments at the Opportunity landing site on Mars. *Nature*, *438*(7071), 1123–1128. https://doi.org/10.1038/nature04383
Kocurek, G. (1988). First-order and super bounding surfaces in aeolian sequences—Bounding surfaces revisited. *Sedimentary Geology*, *56*(1–4), 193–206. https://doi.org/10.1016/0037-0738(88)90054-1
Koeppel, A. H., Edwards, C. S., Annex, A. M., Lewis, K. W., & Carrillo, G. J. (2022). A fragile record of fleeting water on Mars. *Geology*, *50*(2), 152–157. https://doi.org/10.1130/g49285.1
Kokaly, R. F., Clark, R. N., Swayze, G. A., Livo, K. E., Hoefen, T. M., Pearson, N. C., et al. (2017). *USGS spectral library version 7* (Vol. 1035). US Geological Survey.
Komatsu, G., Ori, G. G., Ciarcelluti, P., & Litasov, Y. D. (2004). Interior layered deposits of Valles Marineris, Mars: Analogous subice volcanism related to Baikal Rifting, Southern Siberia. *Planetary and Space Science*, *52*(1–3), 167–187. https://doi.org/10.1016/j.pss.2003.08.003
Komatsu, G., Ori, G. G., Di Lorenzo, S., Rossi, A. P., & Neukum, G. (2007). Combinations of processes responsible for Martian impact crater "layered ejecta structures" emplacement. *Journal of Geophysical Research*, *112*(E6), E06005. https://doi.org/10.1029/2006JE002787
Leask, E. K., Ehlmann, B. L., Dundar, M. M., Murchie, S. L., & Seelos, F. P. (2018). Challenges in the search for perchlorate and other hydrated minerals with 2.1-μm absorptions on Mars. *Journal Geophysical research letters*, *45*(22), 12–180. https://doi.org/10.1029/2018gl080077
Le Deit, L., Hauber, E., Fueten, F., Pondrelli, M., Rossi, A. P., & Jaumann, R. (2013). Sequence of infilling events in Gale Crater, Mars: Results from morphology, stratigraphy, and mineralogy. *Journal of Geophysical Research: Planets*, *118*(12), 2439–2473. https://doi.org/10.1002/2012je004322
Le Deit, L., Le Mouélic, S., Bourgeois, O., Combe, J. P., Mège, D., Sotin, C., et al. (2008). Ferric oxides in east Candor Chasma, Valles Marineris (Mars) inferred from analysis of OMEGA/Mars express data: Identification and geological interpretation. *Journal of Geophysical Research*, *113*(E7), E07001. https://doi.org/10.1029/2007je002950
Lewis, K. W., & Aharonson, O. (2014). Occurrence and origin of rhythmic sedimentary rocks on Mars. *Journal of Geophysical Research: Planets*, *119*(6), 1432–1457. https://doi.org/10.1002/2013je004404
Lewis, K. W., Aharonson, O., Grotzinger, J. P., Kirk, R. L., McEwen, A. S., & Suer, T. A. (2008). Quasi-periodic bedding in the sedimentary rock record of Mars. *Science*, *322*(5907), 1532–1535. https://doi.org/10.1126/science.1161870
Lucchitta, B. K., McEwen, A. S., Clow, G. D., Geissler, P. E., Singer, R. B., Schultz, R. A., & Squyres, S. W. (1992). The canyon system on Mars (pp. 453–492).
Madden, M. E., Bodnar, R. J., & Rimstidt, J. D. (2004). Jarosite as an indicator of water-limited chemical weathering on Mars. *Nature*, *431*(7010), 821–823. https://doi.org/10.1038/nature02971
Malin, M. C. (2007). MRO Context Camera experiment data record level 0 v1.0 [Dataset]. NASA Planetary Data System. https://doi.org/10.17189/1520266
Malin, M. C., Bell, J. F., Cantor, B. A., Caplinger, M. A., Calvin, W. M., Clancy, R. T., et al. (2007). Context camera investigation on board the Mars Reconnaissance Orbiter. *Journal of Geophysical Research*, *112*(E5), E05S04. https://doi.org/10.1029/2006je002808
Malin, M. C., & Edgett, K. S. (2000). Sedimentary rocks of early Mars. *Science*, *290*(5498), 1927–1937. https://doi.org/10.1126/science.290.5498.1927
Malin, M. C., & Edgett, K. S. (2001). Mars global surveyor Mars orbiter camera: Interplanetary cruise through primary mission. *Journal of Geophysical Research*, *106*(E10), 23429–23570. https://doi.org/10.1029/2000je001455
Mangold, N., Ansan, V., Masson, P., & Vincendon, C. (2009). Estimate of aeolian dust thickness in Arabia Terra, Mars: Implications of a thick mantle (>20 m) for hydrogen detection. *Géomorphologie: Relief, Processus, Environnement*, *15*(1), 23–32. https://doi.org/10.4000/geomorphologie.7472

Mangold, N., Dromart, G., Ansan, V., Salese, F., Kleinhans, M. G., Massé, M., et al. (2020). Fluvial regimes, morphometry, and age of Jezero crater paleolake inlet valleys and their exobiological significance for the 2020 Rover Mission Landing Site. *Astrobiology*, *20*(8), 994–1013. https://doi.org/10.1089/ast.2019.2132

Mangold, N., Gendrin, A., Gondet, B., LeMouelic, S., Quantin, C., Ansan, V., et al. (2008). Spectral and geological study of the sulfate-rich region of West Candor Chasma, Mars. *Icarus*, *194*(2), 519–543. https://doi.org/10.1016/j.icarus.2007.10.021

Marcucci, E. C., & Hynek, B. M. (2014). Laboratory simulations of acid-sulfate weathering under volcanic hydrothermal conditions: Implications for early Mars. *Journal of Geophysical Research: Planets*, *119*(3), 679–703. https://doi.org/10.1002/2013je004439

McCollom, T. M., & Hynek, B. M. (2005). A volcanic environment for bedrock diagenesis at Meridiani Planum on Mars. *Nature*, *438*(7071), 1129–1131. https://doi.org/10.1038/nature04390

McCollom, T. M., Hynek, B. M., Rogers, K., Moskowitz, B., & Berquó, T. S. (2013). Chemical and mineralogical trends during acid-sulfate alteration of pyroclastic basalt at Cerro Negro volcano and implications for early Mars. *Journal of Geophysical Research: Planets*, *118*(9), 1719–1751. https://doi.org/10.1002/jgre.20114

McEwen, A. (2007). Mars Reconnaissance Orbiter High Resolution Imaging Science Experiment, reduced data record, MRO-M-HIRISE-3-RDR-V1.1 [Dataset]. NASA Planetary Data System. https://doi.org/10.17189/1520303

McEwen, A. S., Eliason, E. M., Bergstrom, J. W., Bridges, N. T., Hansen, C. J., Delamere, W. A., et al. (2007). Mars Reconnaissance Orbiter's High Resolution Imaging Science Experiment (HiRISE). *Journal of Geophysical Research*, *112*(E5), E05S02. https://doi.org/10.1029/2005je002605

McGuire, P. C., Bishop, J. L., Brown, J. A., Fraeman, A. A., Marzo, G. A., Morgan, M. F., et al. (2009). An improvement to the volcano-scan algorithm for atmospheric correction of CRISM and OMEGA spectral data. *Planetary and Space Science*, *57*(7), 809–815. https://doi.org/10.1016/j.pss.2009.03.007

McLennan, S. M., Bell, J. F., III, Calvin, W. M., Christensen, P. R., Clark, B. D., De Souza, P. A., et al. (2005). Provenance and diagenesis of the evaporite-bearing Burns formation, Meridiani Planum, Mars. *Earth and Planetary Science Letters*, *240*(1), 95–121. https://doi.org/10.1016/j.epsl.2005.09.041

Michalski, J., & Niles, P. B. (2012). Atmospheric origin of Martian interior layered deposits: Links to climate change and the global sulfur cycle. *Geology*, *40*(5), 419–422. https://doi.org/10.1130/g32971.1

Milliken, R. E., Ewing, R. C., Fischer, W. W., & Hurowitz, J. (2014). Wind-blown sandstones cemented by sulfate and clay minerals in Gale Crater, Mars. *Journal of Geophysical Research Letters*, *41*(4), 1149–1154. https://doi.org/10.1002/2013gl059097

Molina, A., López, I., Prieto-Ballesteros, O., Fernández-Remolar, D., de Pablo, M. Á., & Gómez, F. (2017). Coogoon Valles, western Arabia Terra: Hydrological evolution of a complex Martian channel system. *Icarus*, *293*, 27–44. https://doi.org/10.1016/j.icarus.2017.04.002

Montgomery, D. R., Bandfield, J. L., & Becker, S. K. (2012). Periodic bedrock ridges on Mars. *Journal of Geophysical Research*, *117*(E3), E03005. https://doi.org/10.1029/2011JE003970

Moratto, Z. M., Broxton, M. J., Beyer, R. A., Lundy, M., & Husmann, K. (2010). Ames Stereo Pipeline, NASA's open source automated stereogrammetry software. In *Paper presented at 41st Annual Lunar and Planetary Science Conference* (Vol. 1533, p. 2364).

Murana, A. (2018). Geology of Danielson Crater, Mars. *Journal of Maps*, *14*(2), 161–172. https://doi.org/10.1080/17445647.2018.1443029

Murchie, S. (2006). Mars Reconnaissance Orbiter Compact Reconnaissance Imaging Spectrometer for Mars targeted reduced data record, MRO-M-CRISM-3-RDR-TARGETED-V1.0 [Dataset]. NASA Planetary Data System. https://doi.org/10.17189/1519450

Murchie, S., Arvidson, R., Bedini, P., Beisser, K., Bibring, J. P., Bishop, J., et al. (2007). Compact Reconnaissance Imaging Spectrometer for Mars (CRISM) on Mars Reconnaissance Orbiter (MRO). *Journal of Geophysical Research*, *112*(E5), E05S03. https://doi.org/10.1029/2006je002682

Murchie, S., Roach, L., Seelos, F., Milliken, R., Mustard, J., Arvidson, R., et al. (2009). Evidence for the origin of layered deposits in Candor Chasma, Mars, from mineral composition and hydrologic modeling. *Journal of Geophysical Research*, *114*, E00D05. https://doi.org/10.1029/2009JE003343

Murchie, S. L., Seelos, F. P., Hash, C. D., Humm, D. C., Malaret, E., McGovern, J. A., et al. (2009). Compact Reconnaissance Imaging Spectrometer for Mars investigation and data set from the Mars Reconnaissance Orbiter's primary science phase. *Journal of Geophysical Research*, *114*(E2), E00D07. https://doi.org/10.1029/2009je003344

Neukum, G., & Jaumann, R. (2004). HRSC: The high resolution stereo camera of Mars Express. In *Mars Express: The Scientific Payload* (Vol. 1240, pp. 17–35). European Space Agency Special Publication, ESA-SP.

Newsom, H. E., Barber, C. A., Hare, T. M., Schelble, R. T., Sutherland, V. A., & Feldman, W. C. (2003). Paleolakes and impact basins in southern Arabia Terra, including Meridiani Planum: Implications for the formation of hematite deposits on Mars. *Journal of Geophysical Research*, *108*(E12), 8075. https://doi.org/10.1029/2002je001993

Niles, P. B., & Michalski, J. (2009). Meridiani Planum sediments on Mars formed through weathering in massive ice deposits. *Nature Geoscience*, *2*(3), 215–220. https://doi.org/10.1038/ngeo438

Noel, A. J., Bishop, J. L., Al-Samir, M., Gross, C., Flahaut, J., McGuire, P. C., et al. (2015). Mineralogy, morphology and stratigraphy of the light-tones interior layered deposits at Juventae Chasma. *Icarus*, *251*, 315–331. https://doi.org/10.1016/j.icarus.2014.09.033

Oehler, D. Z., & Allen, C. C. (2010). Evidence for pervasive mud volcanism in Acidalia Planitia, Mars. *Icarus*, *208*(2), 636–657. https://doi.org/10.1016/j.icarus.2010.03.031

Pajola, M., Pozzobon, R., Silvestro, S., Salese, F., Rossato, S., Pompilio, L., et al. (2022). Geology, in-situ resource-identification and engineering analysis of the vernal crater area (Arabia Terra): A suitable Mars human landing site candidate. *Planetary and Space Science*, *213*, 105444. https://doi.org/10.1016/j.pss.2022.105444

Pangaea Scientific. (2006–2011). *Orion: Orientation Hunter (computer software)*. Supported by Canada Centre for Remote Sensing, Natural Resources Canada.

Parker, T. J., Gorsline, D. S., Saunders, R. S., Pieri, D. C., & Schneeberger, D. M. (1993). Coastal geomorphology of the Martian northern plains. *Journal of Geophysical Research*, *98*(E6), 11061–11078. https://doi.org/10.1029/93je00618

Pelkey, S. M., Mustard, J. F., Murchie, S., Clancy, R. T., Wolff, M., Smith, M., et al. (2007). CRISM multispectral summary products: Parameterizing mineral diversity on Mars from reflectance. *Journal Geophysical Research*, *112*(E8), E08S14. https://doi.org/10.1029/2006JE002831

Pondrelli, M., Rossi, A. P., Le Deit, L., Fueten, F., van Gasselt, S., Glamoclija, M., et al. (2015). Equatorial layered deposits in Arabia Terra, Mars: Facies and process variability. *GSA Bulletin*, *127*(7–8), 1064–1089.

Pondrelli, M., Rossi, A. P., Le Deit, L., Schmidt, G., Pozzobon, R., Hauber, E., & Salese, F. (2019). Groundwater control and process variability on the equatorial layered deposits of Kotido Crater, Mars. *Journal of Geophysical Research: Planets*, *124*(3), 779–800. https://doi.org/10.1029/2018je005656

Pondrelli, M., Rossi, A. P., Ori, G. G., Van Gasselt, S., Praeg, D., & Ceramicola, S. (2011). Mud volcanoes in the geologic record of Mars: The case of Firsoff crater. *Earth and Planetary Science Letters*, *304*(3–4), 511–519. https://doi.org/10.1016/j.epsl.2011.02.027

Poulet, F., Arvidson, R. E., Gomez, C., Morris, R. V., Bibring, J. P., Langevin, Y., et al. (2008). Mineralogy of Terra Meridiani and western Arabia Terra from OMEGA/MEx and implications for their formation. *Icarus*, *195*(1), 106–130. https://doi.org/10.1016/j.icarus.2007.11.031

Poulet, F., Bibring, J. P., Mustard, J. F., Gendrin, A., Mangold, N., Langevin, Y., et al. (2005). Phyllosilicates on Mars and implications for early Martian climate. *Nature*, *438*(7068), 623–627. https://doi.org/10.1038/nature04274

Pye, K. (1995). The nature, origin and accumulation of loess. *Quaternary Science Reviews*, *14*(7–8), 653–667. https://doi.org/10.1016/0277-3791(95)00047-x

Quantin, C., Allemand, P., Mangold, N., Dromart, G., & Delacourt, C. (2005). Fluvial and lacustrine activity on layered deposits in Melas Chasma, Valles Marineris, Mars. *Journal of Geophysical Research*, *110*(E12), E12S19. https://doi.org/10.1029/2005je002440

Rose, W. I., Riley, C. M., & Dartevelle, S. (2003). Sizes and shapes of 10-Ma distal fall pyroclasts in the Ogallala Group, Nebraska. *The Journal of Geology*, *111*(1), 115–124. https://doi.org/10.1086/344668

Rossi, A. P., Neukum, G., Pondrelli, M., van Gasselt, S., Zegers, T., Hauber, E., et al. (2008). Large-scale spring deposits on Mars? *Journal of Geophysical Research*, *113*(E8), E08016. https://doi.org/10.1029/2007je003062

Ruj, T., Komatsu, G., Dohm, J. M., Miyamoto, H., & Salese, F. (2017). Generic identification and classification of morphostructures in the Noachis-Sabaea region, southern highlands of Mars. *Journal of Maps*, *13*(2), 755–766. https://doi.org/10.1080/17445647.2017.1379913

Salese, F., Ansan, V., Mangold, N., Carter, J., Ody, A., Poulet, F., & Ori, G. G. (2016). A sedimentary origin for intercrater plains north of the Hellas basin: Implications for climate conditions and erosion rates on early Mars. *Journal of Geophysical Research: Planets*, *121*(11), 2239–2267. https://doi.org/10.1002/2016je005039

Salese, F., Di Achille, G., Neesemann, A., Ori, G. G., & Hauber, E. (2016). Hydrological and sedimentary analyses of well-preserved paleofluvial-paleolacustrine systems at Moa Valles, Mars. *Journal of Geophysical Research: Planets*, *121*(2), 194–232. https://doi.org/10.1002/2015je004891

Salese, F., Kleinhans, M. G., Mangold, N., Ansan, V., McMahon, W., De Haas, T., & Dromart, G. (2020). Estimated minimum life span of the Jezero fluvial delta (Mars). *Astrobiology*, *20*(8), 977–993. https://doi.org/10.1089/ast.2020.2228

Salese, F., McMahon, W. J., Balme, M. R., Ansan, V., Davis, J. M., & Kleinhans, M. G. (2020). Sustained fluvial deposition recorded in Mars' Noachian stratigraphic record. *Nature Communications*, *11*(1), 1–8. https://doi.org/10.1038/s41467-020-15622-0

Salese, F., Pondrelli, M., Neeseman, A., Schmidt, G., & Ori, G. G. (2019). Geological evidence of planet-wide groundwater system on Mars. *Journal of Geophysical Research: Planets*, *124*(2), 374–395. https://doi.org/10.1029/2018JE005802

Schmidt, G., Fueten, F., Stesky, R., Flahaut, J., & Hauber, E. (2018). Geology of Hebes Chasma, Mars: 1. Structure, stratigraphy, and mineralogy of the interior layered deposits. *Journal of Geophysical Research: Planets*, *123*(11), 2893–2919. https://doi.org/10.1029/2018je005658

Schmidt, G., Pondrelli, M., Salese, F., Rossi, A. P., Le Deit, L., Fueten, F., & Salvini, F. (2021). Depositional controls of the layered deposits of Arabia Terra, Mars: Hints from basin geometries and stratigraphic trends. *Journal of Geophysical Research: Planets*, *126*(11), e2021JE006974. https://doi.org/10.1029/2021JE006974

Scott, D. H., & Tanaka, K. L. (1982). Ignimbrites of Amazonis Planitia region of Mars. *Journal of Geophysical Research*, *87*(B2), 1179–1190. https://doi.org/10.1029/jb087ib02p01179

Scott, D. H., & Tanaka, K. L. (1986). Geologic map of the western equatorial region of Mars, *US Geological Survey Miscellaneous Investigations Series* (Vol. *1*). scale 1:5000000.

Segura, T. L., Toon, O. B., Colaprete, A., & Zahnle, K. (2002). Environmental effects of large impacts on Mars. *Science*, *298*(5600), 1977–1980. https://doi.org/10.1126/science.1073586

Shean, D. E., Alexandrov, O., Moratto, Z. M., Smith, B. E., Joughin, I. R., Porter, C., & Morin, P. (2016). An automated, open-source pipeline for mass production of digital elevation models (DEMs) from very-high-resolution commercial stereo satellite imagery. *ISPRS Journal of Photogrammetry and Remote Sensing*, *116*, 101–117. https://doi.org/10.1016/j.isprsjprs.2016.03.012

Silvestro, S., Pacifici, A., Salese, F., Vaz, D. A., Neesemann, A., Tirsch, D., et al. (2021). Periodic Bedrock Ridges at the ExoMars 2022 landing site: Evidence for a changing wind regime. *Journal of Geophysical research letters*, *48*(4), e2020GL091651. https://doi.org/10.1029/2020gl091651

Skok, J. R., Mustard, J. F., Tornabene, L. L., Pan, C., Rogers, D., & Murchie, S. L. (2012). A spectroscopic analysis of Martian crater central peaks: Formation of the ancient crust. *Journal of Geophysical Research*, *117*(E11), E00J18. https://doi.org/10.1029/2012je004148

Smith, D. E. (1999). Mola Initial experiment gridded data record, MGS-M-MOLA-5-IEGDR-L3-V2.0 [Dataset]. NASA Planetary Data System. https://doi.org/10.17189/1519447

Smith, D. E., Zuber, M. T., Frey, H. V., Garvin, J. B., Head, J. W., Muhleman, D. O., et al. (2001). Mars Orbiter Laser Altimeter: Experiment summary after the first year of global mapping of Mars. *Journal of Geophysical Research*, *106*(E10), 23689–23722. https://doi.org/10.1029/2000je001364

Squyres, S. W., Grotzinger, J. P., Arvidson, R. E., Bell, J. F., Calvin, W., Christensen, P. R., et al. (2004). In situ evidence for an ancient aqueous environment at Meridiani Planum, Mars. *Science*, *306*(5702), 1709–1714. https://doi.org/10.1126/science.1104559

Squyres, S. W., & Knoll, A. H. (2005). Sedimentary rocks at Meridiani Planum: Origin, diagenesis, and implications for life on Mars. *Earth and Planetary Science Letters*, *240*(1), 1–10. https://doi.org/10.1016/j.epsl.2005.09.038

Squyres, S. W., Knoll, A. H., Arvidson, R. E., Ashley, J. W., Bell, J. F., Calvin, W. M., et al. (2009). Exploration of Victoria crater by the Mars rover Opportunity. *Science*, *324*(5930), 1058–1061. https://doi.org/10.1126/science.1170355

Sutton, S. S., Chojnacki, M., McEwen, A. S., Kirk, R. L., Dundas, C. M., Schaefer, E. I., et al. (2022). Revealing active Mars with HiRISE digital terrain models. *Remote Sensing*, *14*(10), 2403. https://doi.org/10.3390/rs14102403

Tanaka, K. L. (2000). Dust and ice deposition in the Martian geologic record. *Icarus*, *144*(2), 254–266. https://doi.org/10.1006/icar.1999.6297

Tanaka, K. L., Skinner, J. A., Jr., Dohm, J. M., Irwin, R. P., III, Kolb, E. J., Fortezzo, C. M., et al. (2014). *Geologic map of Mars* (pp. 32–92). USGS Geological Survey Scientific Investigations Map.

Vago, J., Witasse, O., Svedhem, H., Baglioni, P., Haldemann, A., Gianfiglio, G., et al. (2015). ESA ExoMars program: The next step in exploring Mars. *Solar System Research*, *49*(7), 518–528. https://doi.org/10.1134/s0038094615070199

Vaniman, D. T., Bish, D. L., Chipera, S. J., Fialips, C. I., Carey, J. W., & Feldman, W. C. (2004). Magnesium sulfate salts and the history of water on Mars. *Nature*, *431*(7009), 663–665. https://doi.org/10.1038/nature02973

Verosub, K. L., Fine, P., Singer, M. J., & TenPas, J. (1993). Pedogenesis and paleoclimate: Interpretation of the magnetic susceptibility record of Chinese loess-paleosol sequences. *Geology*, *21*(11), 1011–1014. https://doi.org/10.1130/0091-7613(1993)021<1011:papiot>2.3.co;2

Viviano, C. E., Seelos, F. P., Murchie, S. L., Kahn, E. G., Seelos, K. D., Taylor, H. W., et al. (2014). Revised CRISM spectral parameters and summary products based on the currently detected mineral diversity on Mars. *Journal of Geophysical Reesearch: Planets*, *119*(6), 1403–1431. https://doi.org/10.1002/2014je004627

Wang, A., Freeman, J. J., & Jolliff, B. L. (2009). Phase transition pathways of the hydrates of magnesium sulfate in the temperature range 50°C to 5°C: Implication for sulfates on Mars. *Journal of Geophysical Research*, *114*(E4), E04010. https://doi.org/10.1029/2008je003266

Wilhelms, D. E. (1976). Geologic map of the Oxia Palus quadrangle of Mars. *US Geological Survey Report* (Vol. *895*).

Wilson, S. A., Howard, A. D., Moore, J. M., & Grant, J. A. (2007). Geomorphic and stratigraphic analysis of Crater Terby and layered deposits north of Hellas basin, Mars. *Journal of Geophysical Research*, *112*(E8), E08009. https://doi.org/10.1029/2006je002830

Wiseman, S. M., Arvidson, R. E., Morris, R. V., Poulet, F., Andrews-Hanna, J. C., Bishop, J. L., et al. (2010). Spectral and stratigraphic mapping of hydrated sulfate and phyllosilicate-bearing deposits in northern Sinus Meridiani, Mars. *Journal of Geophysical Research*, *115*(E7), E00D18. https://doi.org/10.1029/2009je003354

Zabrusky, K., Andrews-Hanna, J. C., & Wiseman, S. M. (2012). Reconstructing the distribution and depositional history of the sedimentary deposits of Arabia Terra, Mars. *Icarus*, *220*(2), 311–330. https://doi.org/10.1016/j.icarus.2012.05.007

Zabrusky, K. J., & Andrews-Hanna, J. C. (2010). Reconstructing the original volume and extent of the sedimentary deposits of Meridiani Planum and Arabia Terra. In *Paper presented at 41st Annual Lunar and Planetary Science Conference* (Vol. 1533, p. 2529).

Zuber, M. T. (2001). The crust and mantle of Mars. *Nature*, *412*(6843), 220–227. https://doi.org/10.1038/35084163